Supporting Information for

Spectroscopic and DFT Characterization of a Highly Reactive Nonheme Fe^{V}-oxo Intermediate

Ruixi Fan,[†,&] Joan Serrano-Plana,[‡,&] Williamson N. Oloo,[§] Apparao Draksharapu,[§] Estefanía Delgado-Pinar,[¥] Anna Company,[‡] Vlad Martin-Diaconescu,[‡] Margarida Borrell,[‡] Julio Lloret-Fillol,[‖] Enrique García-España,*[,¥] Yisong Guo,*[,†] Emile L. Bominaar,*[,†] Lawrence Que Jr.,*[,§] Miquel Costas,*[,‡] and Eckard Münck*[,†]

[†]Department of Chemistry, Carnegie Mellon University, 4400 Fifth Avenue, Pittsburgh, Pennsylvania 15213, United States

[‡]Grup de Química Bioinspirada, Supramolecular i Catàlisi (QBIS-CAT), Institut de Química Computacional i Catàlisi (IQCC), Departament de Química, Universitat de Girona, C/M. Aurèlia Capmany 69, 17003 Girona, Catalonia, Spain

[§]Department of Chemistry and Center for Metals in Biocatalysis, University of Minnesota, Minneapolis, Minnesota 55455, United States

[‖]Institute of Chemical Research of Catalonia (ICIQ), The Barcelona Institute of Science and Technology, Avinguda Països Catalans 16, 43007, Tarragona, Spain.

[¥]Grup de Química Supramolecular, Institut de Ciència Molecular, Departament de Química Inorgànica, Universitat de València, 46980, Paterna, (Valencia), Spain

[&]R.F. and J.S.-P. made equal contributions to this work.

Contents

I. Synthesis and characterization of [(MeO-PyNMe$_3$)Fe^{II}(CF$_3$SO$_3$)$_2$]

The following compounds were prepared according to literature procedures.[1]

Dimethyl-4-hydroxypyridine-2,6-dicarboxylate (HO-PyCOOMe)

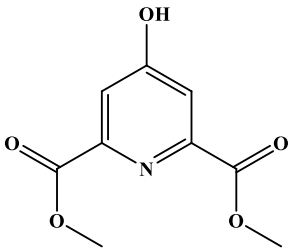

Commercially available chelidamic acid hydrate (3 g, 14.91 mmol) was suspended in dry methanol (40 mL), and concentrated sulfuric acid (500 µL, 9.37 mmol) was added. The solution was heated at reflux for 4 h under stirring and then the solvent was evaporated until dryness. The crude product was dissolved in 200 mL of a saturated solution of $NaHCO_3$(aq) and washed with EtOAc (4x50 mL). The combined organic layers were dried over Na_2SO_4 and concentrated until a white solid is obtained (4.97 g). Yield: 92%. ^{1}H NMR (300 MHz, DMSO) δ(ppm): 7.59 (s, 2H), 3.90 (s, 6H). (Sometimes a small amount of MeO-PyCOOMe appears in this step together with HO-PyCOOMe.)

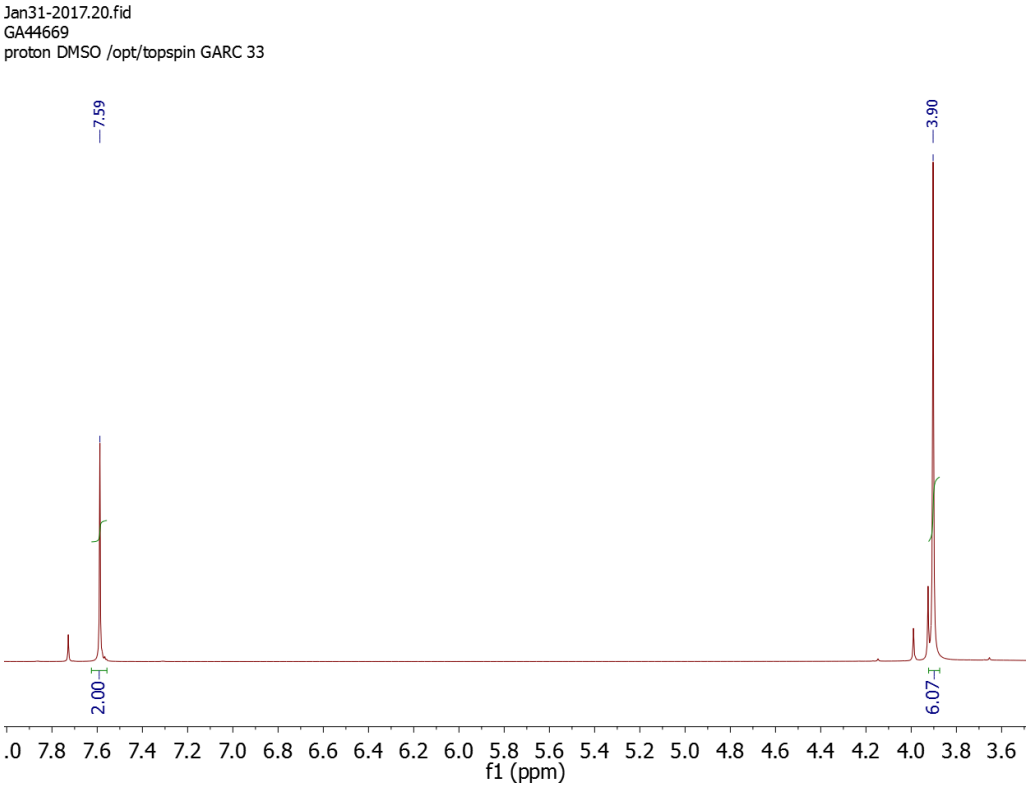

Figure S1. ^{1}H-NMR spectrum of HO-PyCOOMe in d_6-DMSO at 298 K.

Dimethyl-4-methoxypyridine-2,6-dicarboxylate (MeO-PyCOOMe)

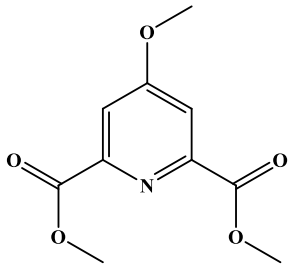

HO-PyCOOMe (5.0 g, 24.11 mmol) was dissolved in CH_3CN (50 mL) and K_2CO_3 (4.96 g, 36.12 mmol) was added to the solution. Then, methyl iodide (5.12 mL, 36.12mmol) was added and the mixture was refluxed under N2 atmosphere and stirred for 24 hours. The reaction mixture was cooled to room temperature and water was then added. The solvent was evaporated under reduced pressure and the aqueous layer was extracted with CH_2Cl_2. Organic layers were dried over Na_2SO_4 and concentrated until a white solid was obtained (4.58 g). Yield: 86.2%. ^{1}H NMR (300 MHz, $CDCl_3$) δ(ppm): 7.82 (s, 2H), 4.01 (s, 6H), 3.99 (s, 3H). ^{13}C NMR (75 MHz, $CDCl_3$) δ(ppm): 167.73, 165.22, 149.87, 114.24, 56.16, 53.34.

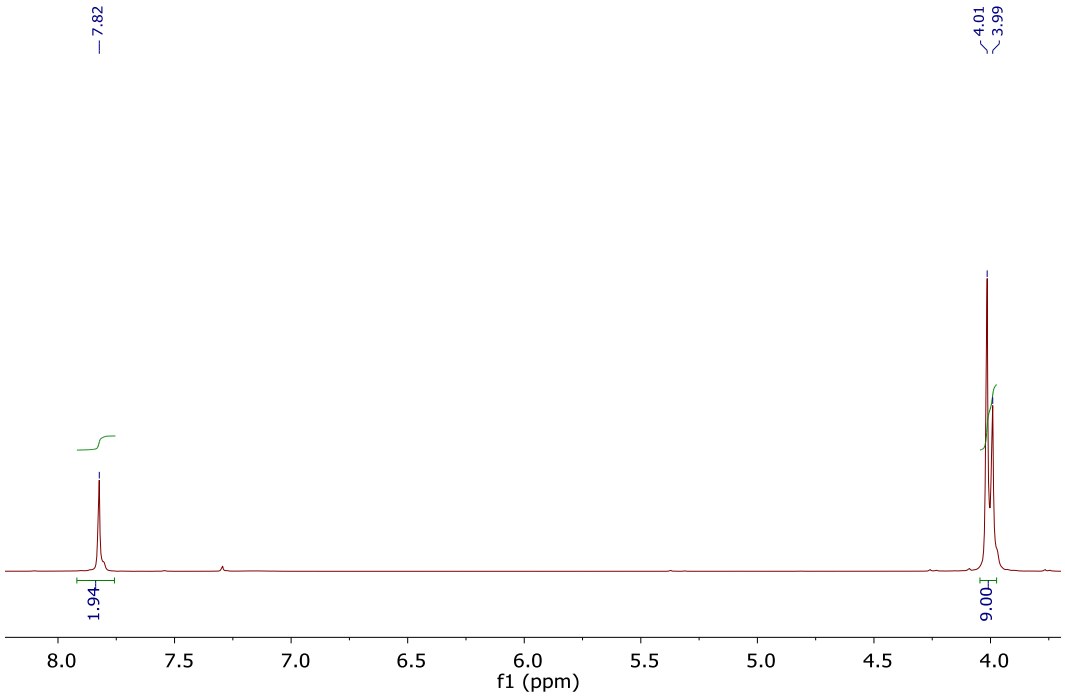

Figure S2. ^{1}H-NMR spectrum of MeO-PyCOOMe in $CDCl_3$ at 298 K.

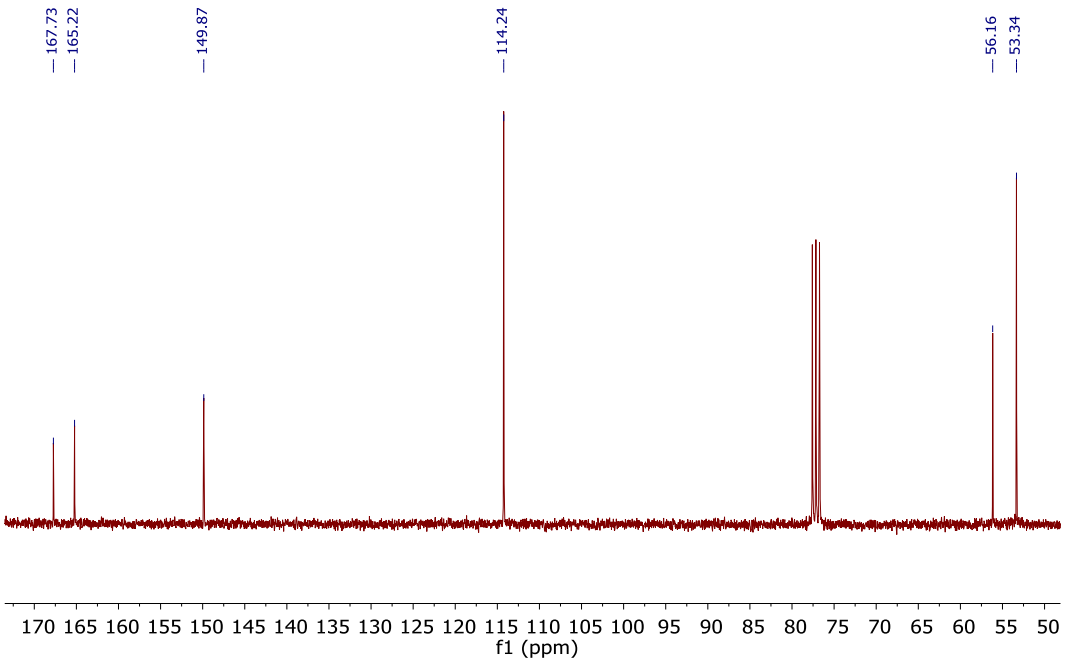

Figure S3. ^{13}C-NMR spectrum of MeO-PyCOOMe in $CDCl_3$ at 298 K.

2.6-Dihydroxymethyl-4-methoxypyridine (MeO-PyOH)

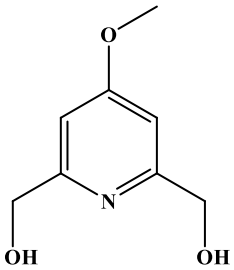

MeO-PyCOOMe (2.13 g, 9.45 mmol) was dissolved in dry ethanol (100 mL) and $NaBH_4$ (1.60 g, 42.29 mmol) was added in small portions over a period of 30 min. The reaction mixture was refluxed under N_2 atmosphere for 24 h, the solvent was removed under vacuum and a concentrated solution of $NaHCO_3$ was added. The reaction mixture was refluxed for an additional 2 h and the aqueous layer was extracted with EtOAc. Organic layers were dried over Na_2SO_4 and concentrated until a white solid was obtained (2.13 g). Yield: 96.25%. ^{1}H NMR (300 MHz, MeOD) δ(ppm): 6.97 (s, 2H), 4.61 (s, 4H), 3.89 (s, 3H). ^{13}C NMR (75 MHz, MeOD) δ(ppm): 169.41, 163.65, 105.95, 65.24, 55.89.

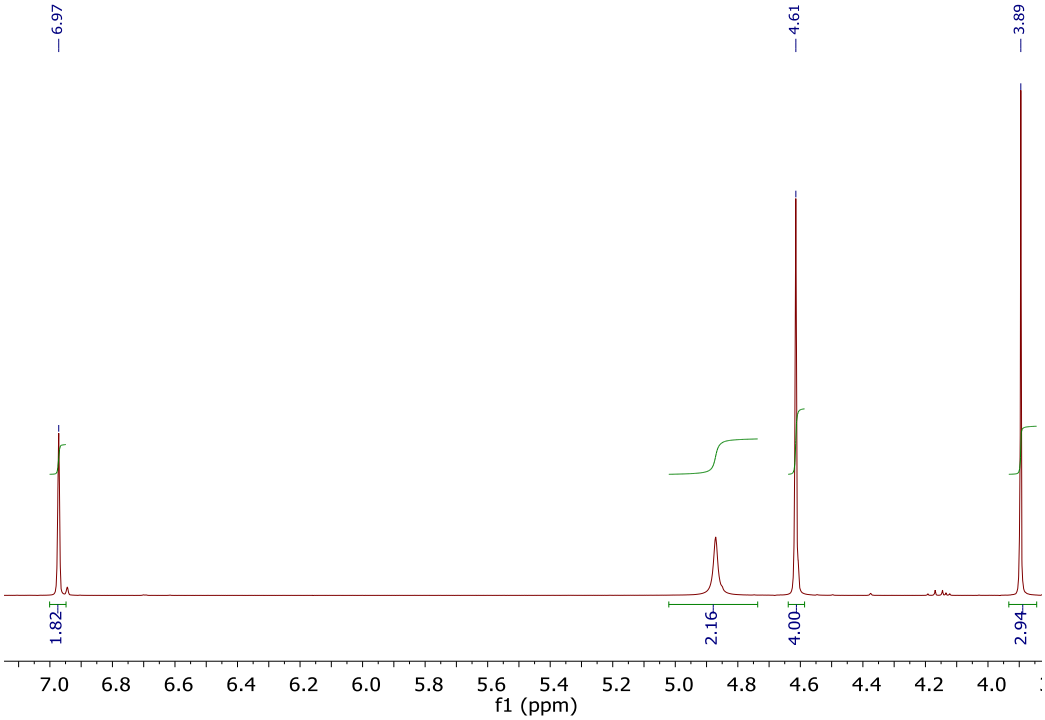

Figure S4. ^{1}H-NMR spectrum of MeO-PyOH in MeOD at 298 K.

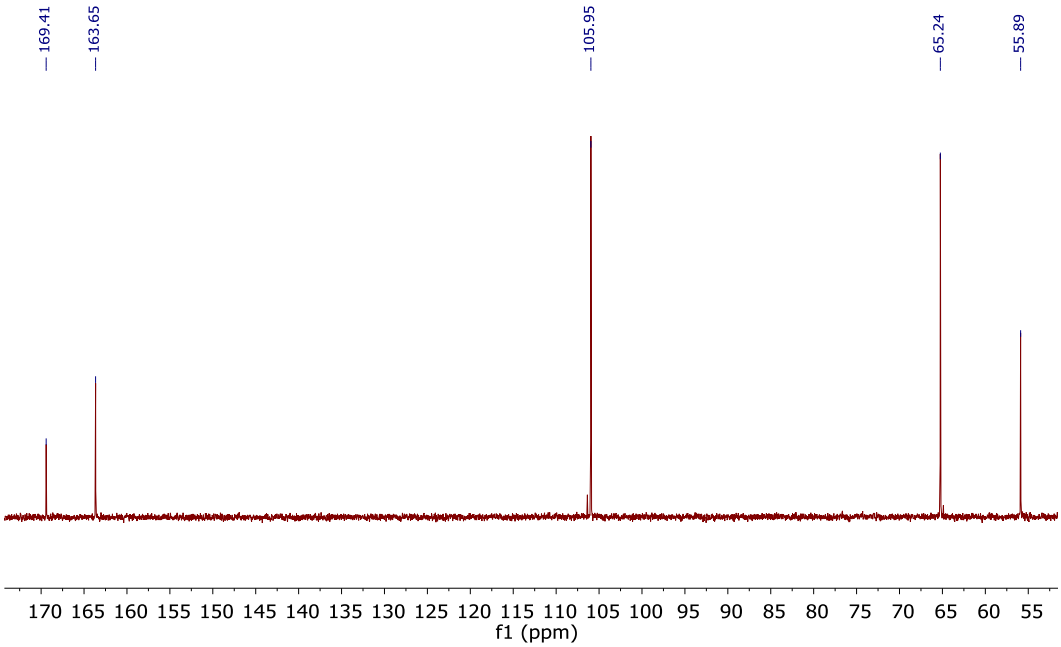

Figure S5. ^{13}C-NMR spectrum of MeO-PyOH in MeOD at 298 K.

2,6-Dibromomethyl-4-methoxypyridine (MeO-PyBr)[2]

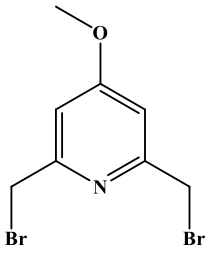

A suspension of MeO-PyOH (1.13 g, 6.78 mmol) in $CHCl_3$ (50 mL) was cooled in an iced-bath and then PBr_3 (9.71 mL, 103.33 mmol) was added dropwise. The reaction mixture was stirred for 2 hours and then refluxed for 12 hours. The cooled mixture was neutralized with concentrated $NaHCO_3$ (aq) and the organic layer was separated. The aqueous layer was extracted with chloroform twice. The combined organic phases were dried with Na_2SO_4 and the solvent was evaporated under vacuum. The compound MeO-PyBr was then purified on column chromatography (CH_2Cl_2/Acetone; 99:1) as a white solid 1.53 g. Yield: 78%. ^{1}H NMR (300 MHz, $CDCl_3$) δ(ppm): 6.89 (s, 2H), 4.48 (s, 4H), 3.88 (s, 3H). ^{13}C NMR (75 MHz, $CDCl_3$) δ(ppm): 167.38, 158.35, 109.06, 55.63, 33.71. ESI-MS (m/z): Found: 317.7 $[M + Na]^+$ (100%); Theoretical: 317.97 $[M + Na]^+$ (100%).

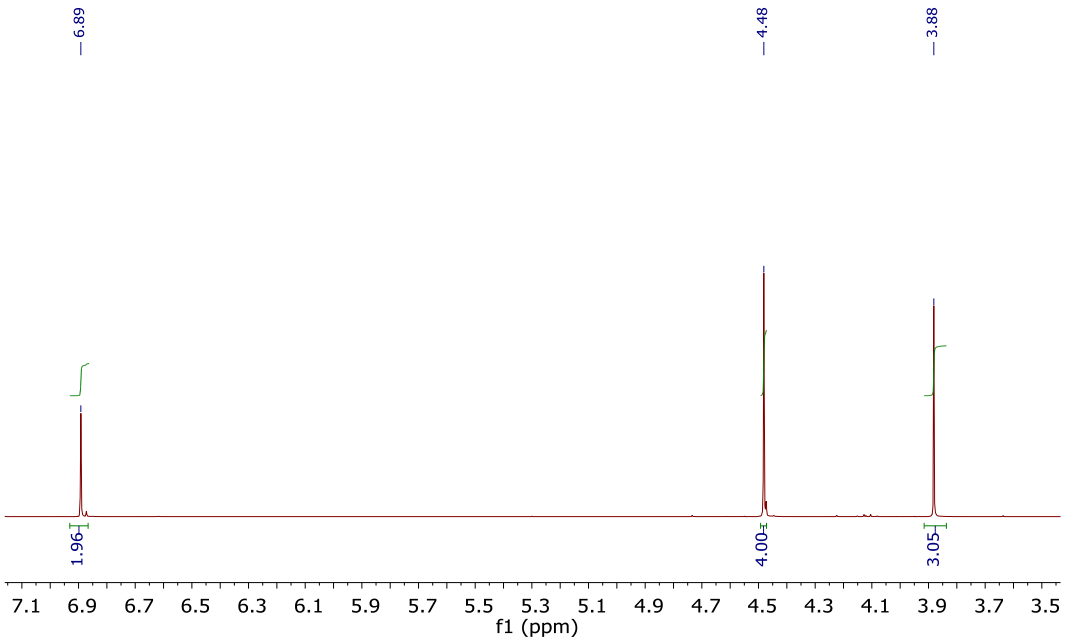

Figure S6. ^{1}H-NMR spectrum of MeO-PyBr in $CDCl_3$ at 298 K.

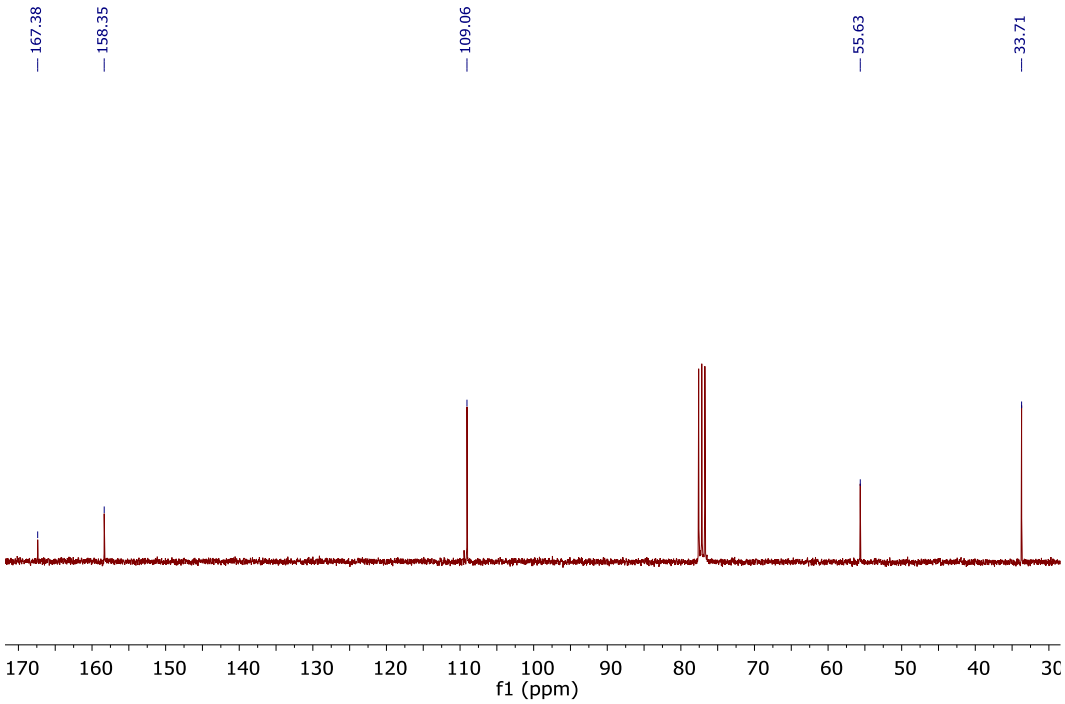

Figure S7. ^{13}C-NMR spectrum of MeO-PyBr in $CDCl_3$ at 298 K.

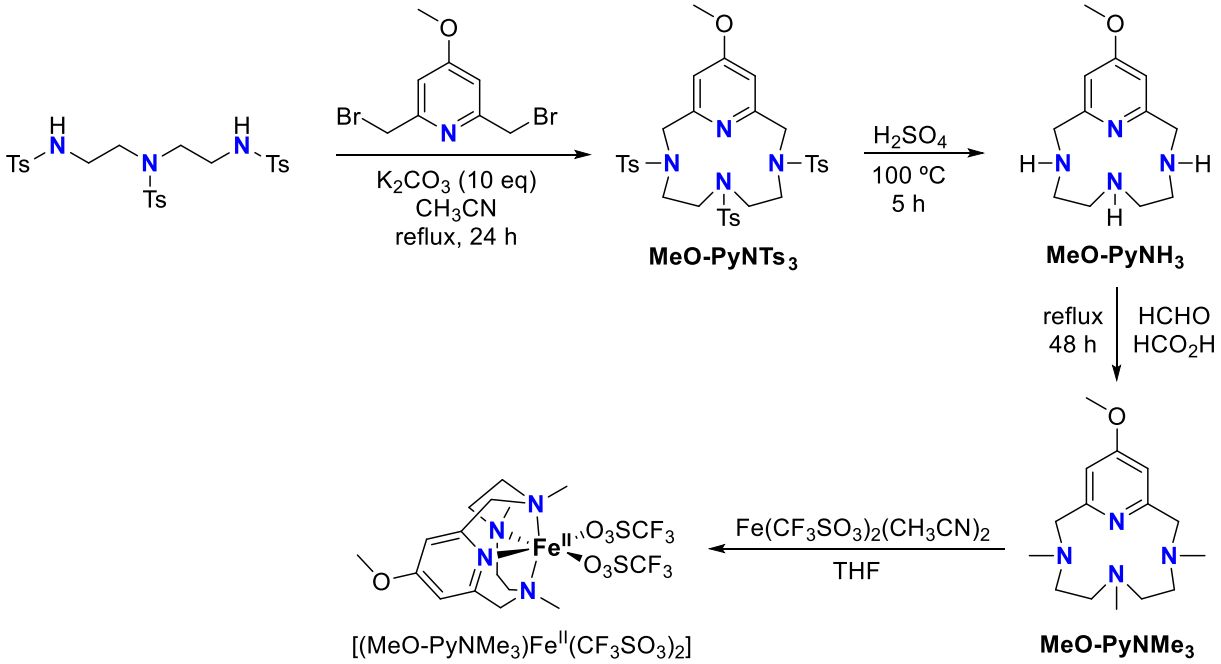

Scheme S1. Synthetic route for the preparation of MeO-PyNMe$_3$ and [(MeO-PyNMe$_3$)Fe^{II}(CF$_3$SO$_3$)$_2$] complex.[3]

MeO-PyNTs$_3$

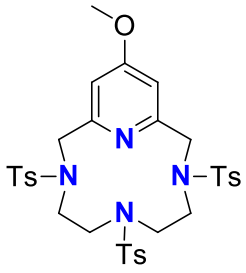

N,N',N''-tris(p-toluenesufonyl)diethylenetriamine (2.68 g, 4.74 mmol) and potassium carbonate (6.56 g, 138.21 mmol) were introduced in a two necked round-bottom flask and CH_3CN (300 mL) was added. After heating the mixture to reflux, a solution of 2,6-dibromomethyl-4-methoxypyridine (1.4 g, 4.74 mmol) in CH_3CN (100 mL) was added dropwise over a period of 2 hours. The mixture was stirred at 100 ºC under N_2 atmosphere overnight and then cooled down to room temperature. After filtration, the solvent was removed under reduced pressure, obtaining a yellow solid. MeO-PyNTs$_3$ was purified by column chromatography over silica (95:5; CH_2Cl_2:Acetone). MeO-PyNTs3 (4.61 g) was obtained pure as a white solid. Yield: 73%. ^{1}H NMR (300 MHz, $CDCl_3$) δ (ppm): 7.70/7.73 (d, J = 8.30 Hz, 4H), 7.65/7.68 (d, J = 8.30 Hz, 2H), 7.33/7.35 (d, J = 7.95 Hz, 4H), 7.27/7.29 (d, J = 8.00 Hz, 2H), 6.90 (s, 2H), 4.22 (s, 4H), 3.58 (s, 3H), 3.32 (t, J = 7.63 Hz, 4H), 2.80 (broad s, 4H), 2.44 (s, 6H), 2.41 (s, 3H). ^{13}C NMR (75 MHz, $CDCl_3$) δ (ppm): 168.26, 157.07, 144.17, 143.86, 136.42, 135.66, 130.33, 130.20, 127.59, 127.51, 110.63, 56.03, 55.39, 50.51, 47.65, 21.94.

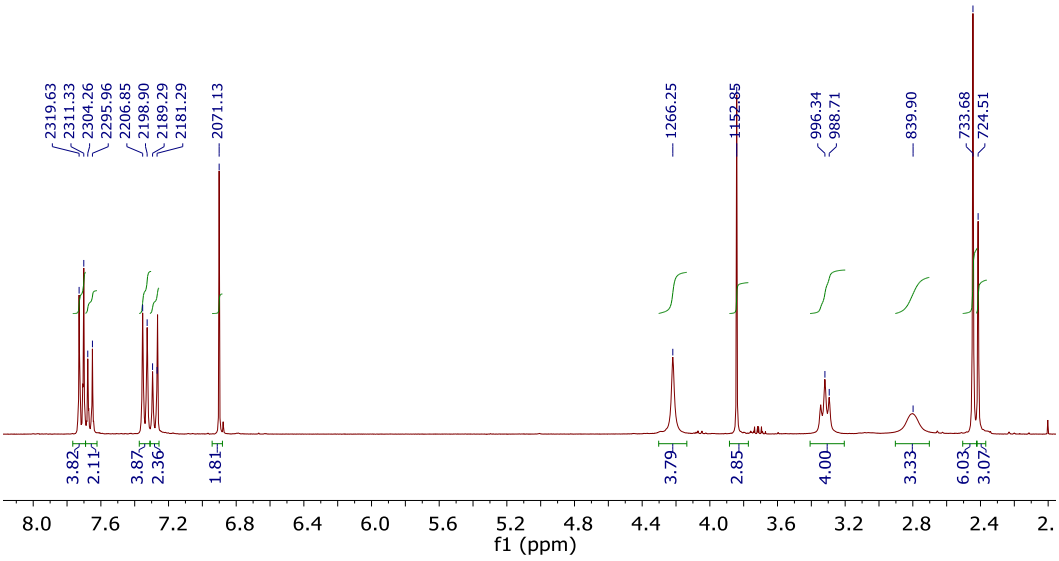

Figure S9. ^{1}H-NMR spectrum of MeO-PyNTs$_3$ in $CDCl_3$ at 298 K.

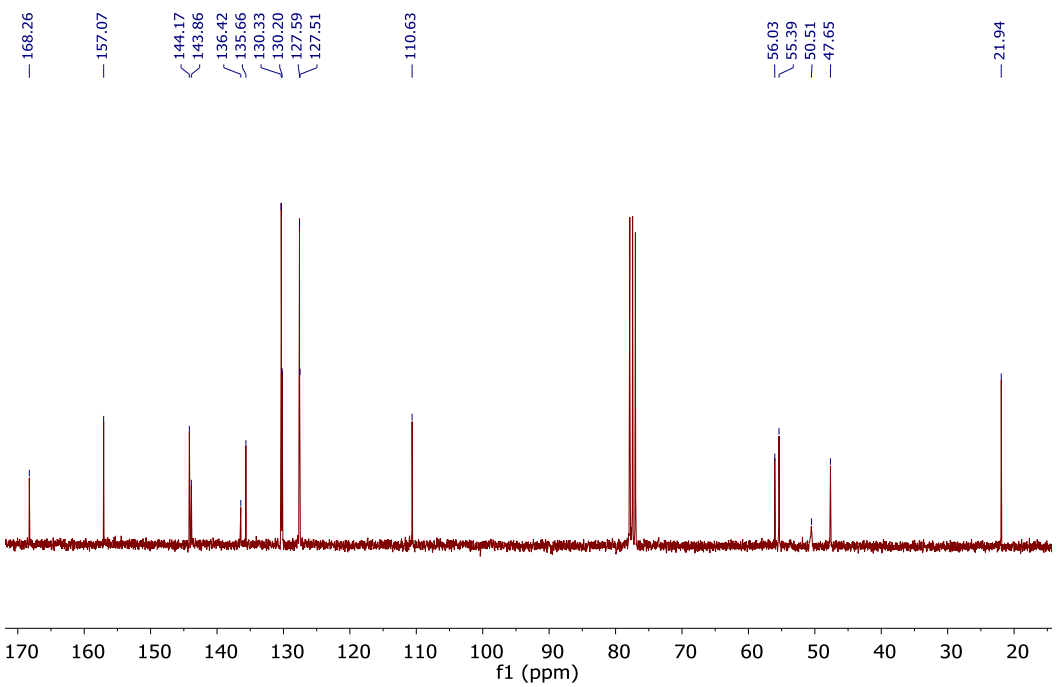

Figure S10. ^{13}C-NMR spectrum of MeO-PyNTs$_3$ in $CDCl_3$ at 298 K.

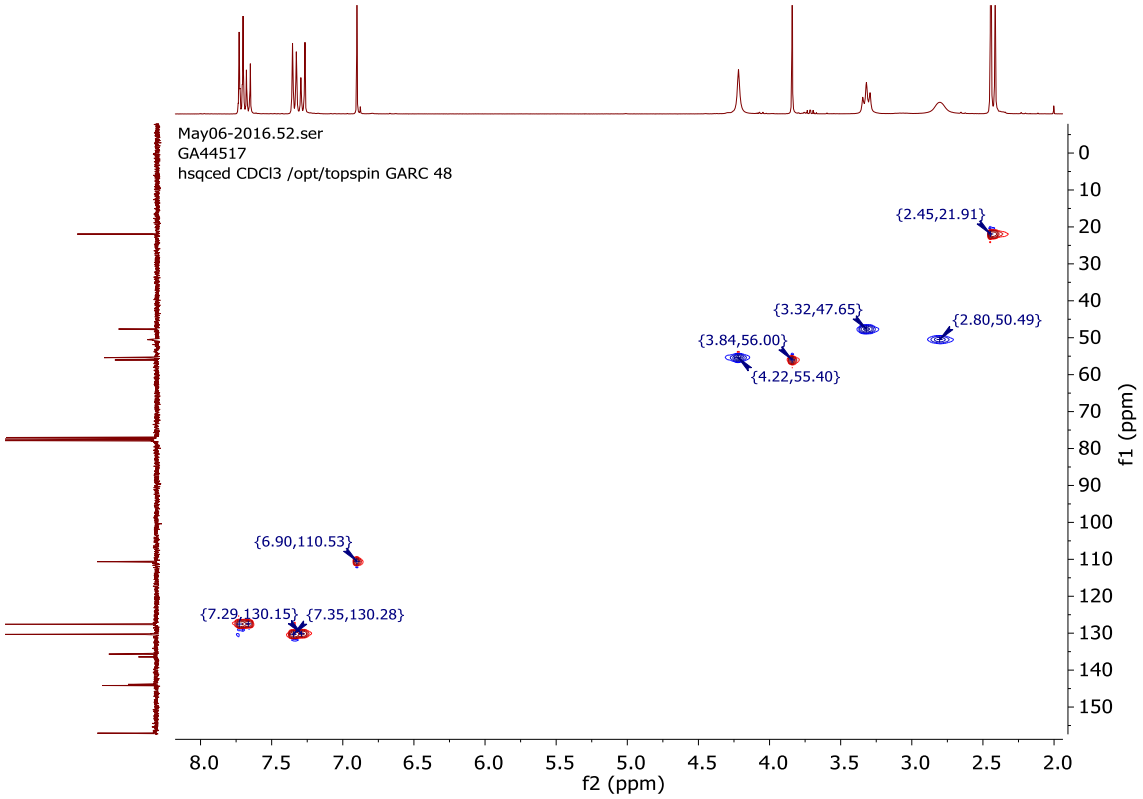

Figure S11. HSQC-NMR spectrum of MeO-PyNTs$_3$ in $CDCl_3$ at 298 K.

MeO-PyNH$_3$[4]

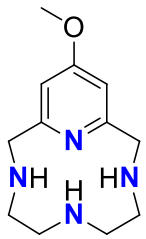

A solution of MeO-PyNTs$_3$ (1.09 g, 1.56 mmol) in conc. H_2SO_4 (19.14 mL, 34.82 mmol) was stirred at 100 °C for 5 h. The dark brown solution was cooled to room temperature, placed in an ice-bath and an excess concentrated NaOH aqueous solution was then added. The aqueous phase was extracted with $CHCl_3$ (3 x 50 mL), the combined organic phases were dried with Na_2SO_4 and the solvent was evaporated under vacuum affording a pale yellow oil that was used in the next step without further purification. Yield: 70%. ^{1}H NMR (300 MHz, CDCl3) δ (ppm): 6.54 (s, 2H), 3.90 (s, 4H), 3.84 (s, 3H), 3.56 (broad s, 3H), 2.74 (t, J = 5.67 Hz, 4H), 2.27-230 (m, 4H). ^{13}C-DEPT NMR (75 MHz, $CDCl_3$) δ (ppm): 106.11, 55.44, 54.26, 49.20, 48,96. ESI-MS (m/z): Found: 236.9 [M]+ (100%); Theoretical: 237.17[M]+ (100%).

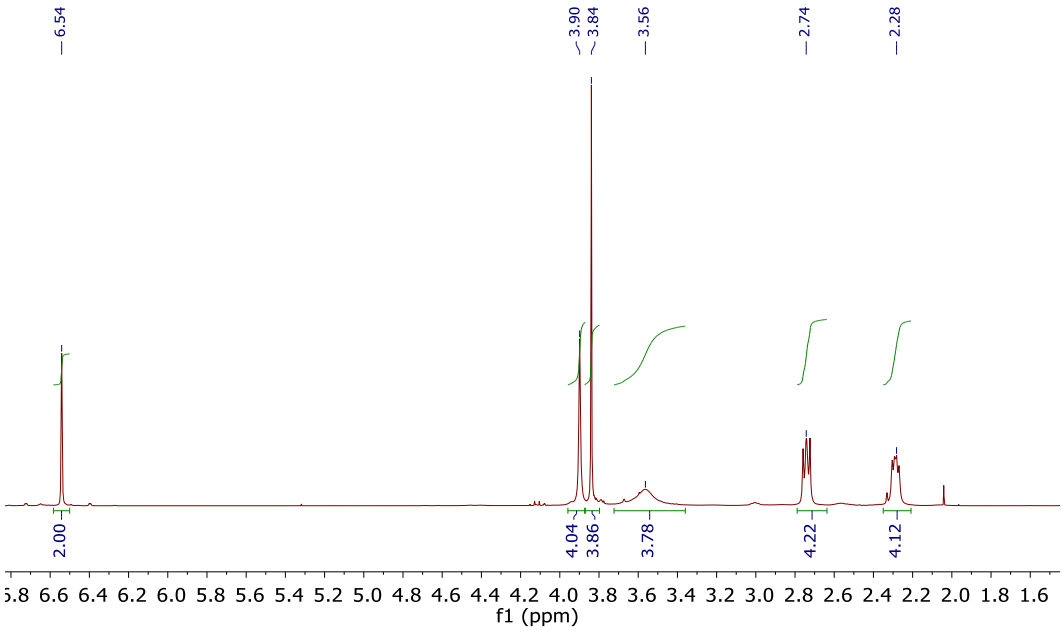

Figure S12. ^{1}H-NMR spectrum of MeO-PyNH$_3$ in $CDCl_3$ at 298 K.

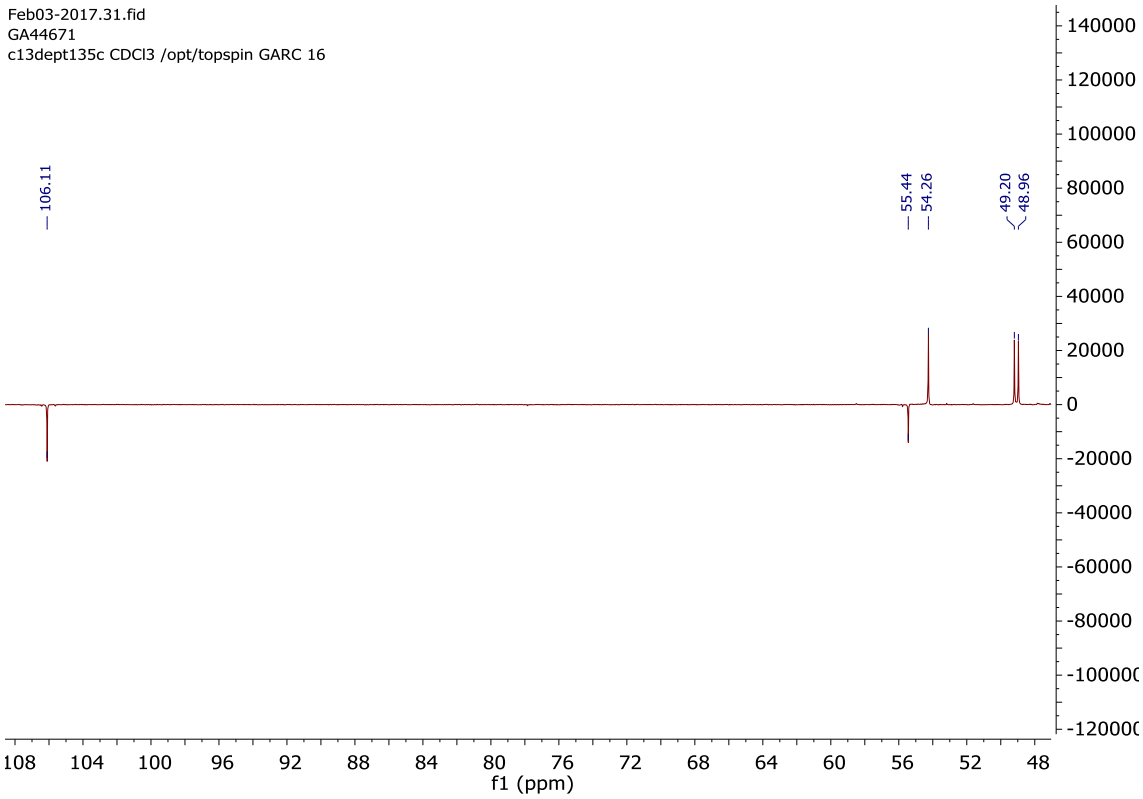

Figure S13. DEPT-NMR spectrum of MeO-PyNH$_3$ in CDCl$_3$ at 298 K.

MeO-PyNMe$_3$

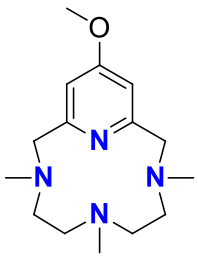

MeO-PyNH$_3$ (0.320 g, 1.35 mmol) was dissolved in formic acid (1.24 mL, 28.45 mmol) and formaldehyde 37% (1.02 mL, 12.22 mmol) in a 10 mL round flask. After the addition of 116 µL of water, the resulting mixture was refluxed for 48 hours. The solution was cooled to room temperature, placed in an ice-bath and neutralized with conc. $NaHCO_3$ (aq). The aqueous phase was extracted with CH_2Cl_2 (3 x 50 mL), the combined organic phases were dried with Na2SO4 and the solvent was evaporated under vacuum affording a yellow oil which was purified by alumina column chromatography (CH_2Cl_2:MeOH 93:7) obtaining 0.27 mg. Yield: 70%. ^{1}H NMR (300 MHz, $CDCl_3$) δ (ppm): 6.60 (s, 2H), 3.88 (s, 3H), 3.72 (s, 4H), 3.30 (broad s, 4H), 2.97 (s, 3H), 2.97 (t, J = 5.93 Hz, 4H), 2.58 (6, 6H). ^{13}C NMR (75 MHz, $CDCl_3$) δ (ppm): 167.11, 160.44, 106.37, 60.26, 55.53, 54.62, 52.25, 45.54, 36.83. ESI-MS (m/z): Found: 279.0 $[M]^+$ (100%); Theoretical: 279.21 $[M]^+$ (100%).

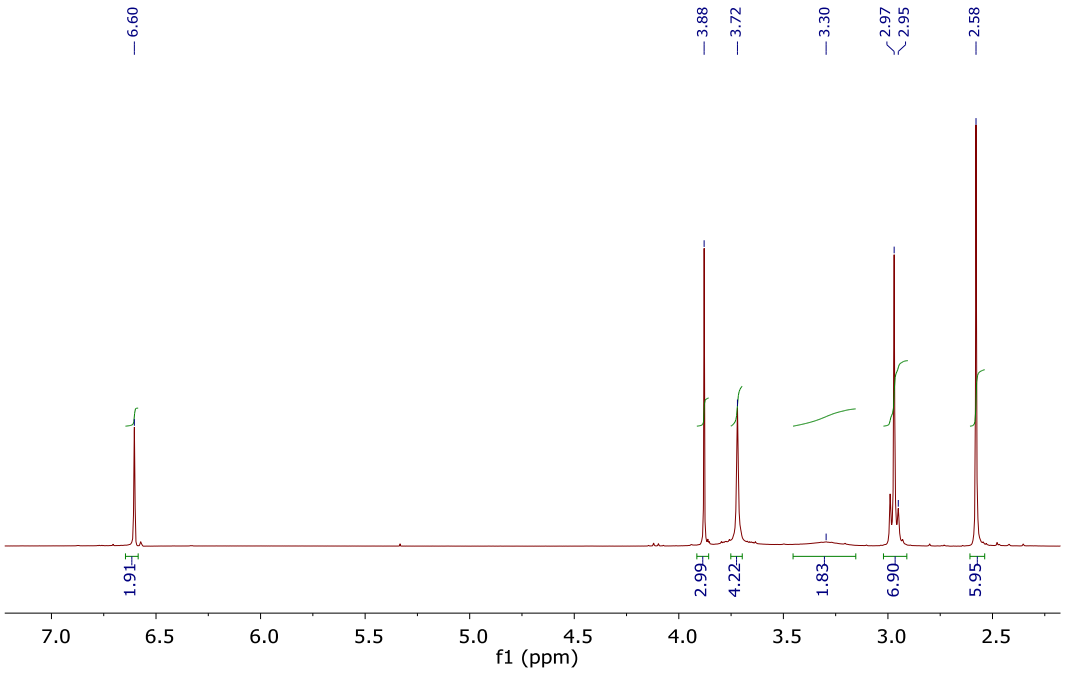

Figure S14. ^{1}H-NMR spectrum of MeO-PyNMe$_3$ in $CDCl_3$ at 298 K.

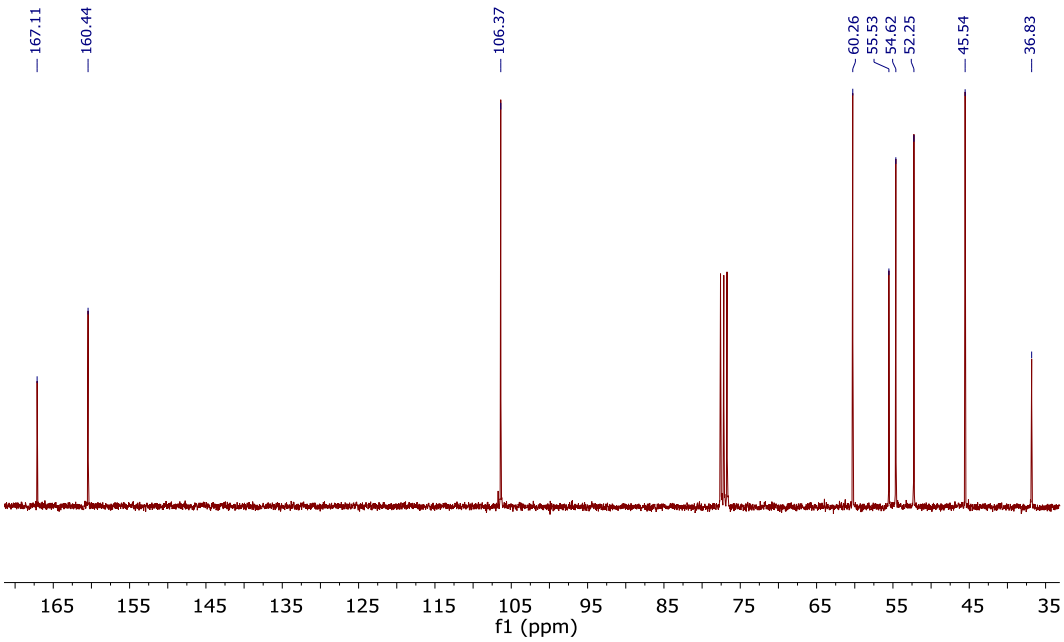

Figure S15. ^{13}C-NMR spectrum of MeO-PyNMe$_3$ in CDCl$_3$ at 298 K.

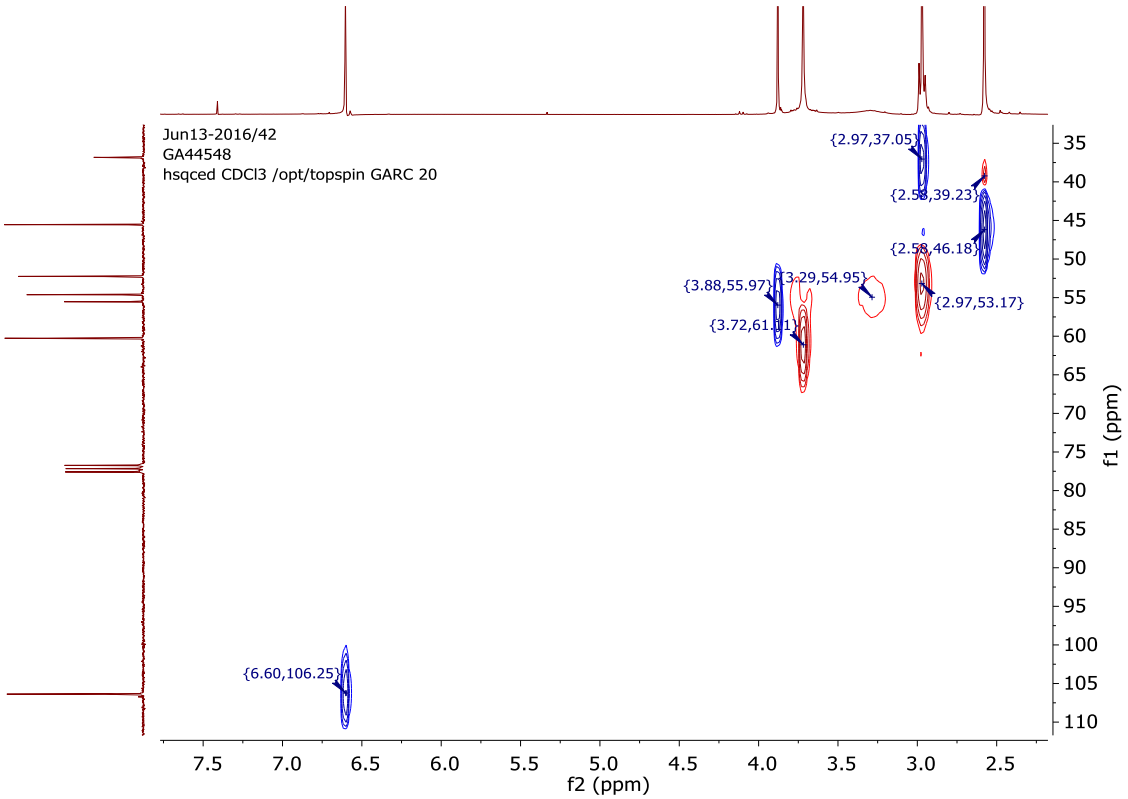

Figure S16. HSQC-NMR spectrum of MeO-PyNMe$_3$ in CDCl$_3$ at 298 K.

[(MeO-PyNMe$_3$)Fe^{II}(CF$_3$SO$_3$)$_2$]

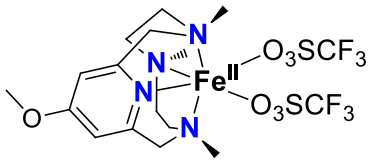

MeO-PyNMe$_3$ (27.2 mg, 97.8 mmols) was dissolved in THF (1 mL) and a solution of [Fe(CF$_3$SO$_3$)$_2$(CH$_3$CN)$_2$] (42.6 mg, 97.8 mmols) in THF (1 mL) was added dropwise under inert atmosphere. After ~2 min a white precipitate started to appear and the mixture was left stirring for further 2 hours. Then the solid was separated and washed with THF and afterwards dried under vacuum. The resulting solid was redissolved in 2 mL CH_2Cl_2 and a few drops of CH_3CN. After diffusion with diethyl ether, 63 mg (100 mmols, 63% yield) of pale brown crystals suitable for X-Ray analysis were obtained. ^{1}H-NMR (CD_3CN, 298 MHz, 298 K) δ, ppm = 128.2, 116.9, 110.4, 91.5, 83.3, 77.1, 70.1, 63.0, 60.46, 53.5, -1.7, -3.5, -18.1, -23.3. HR-MS (ESI-TOF) m/z: calc for [[Fe($C_{15}H_{26}N_4O$)](CF$_3$SO$_3$)]$^+$ 483.0971 found 483.0986.

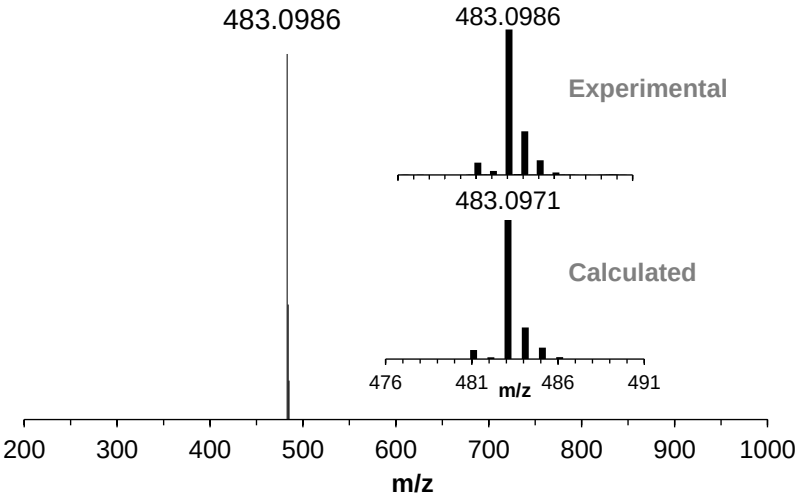

Figure S17. High resolution mass spectrum (HR-MS) of [(MeO-PyNMe$_3$)Fe^{II}(CF$_3$SO$_3$)$_2$].

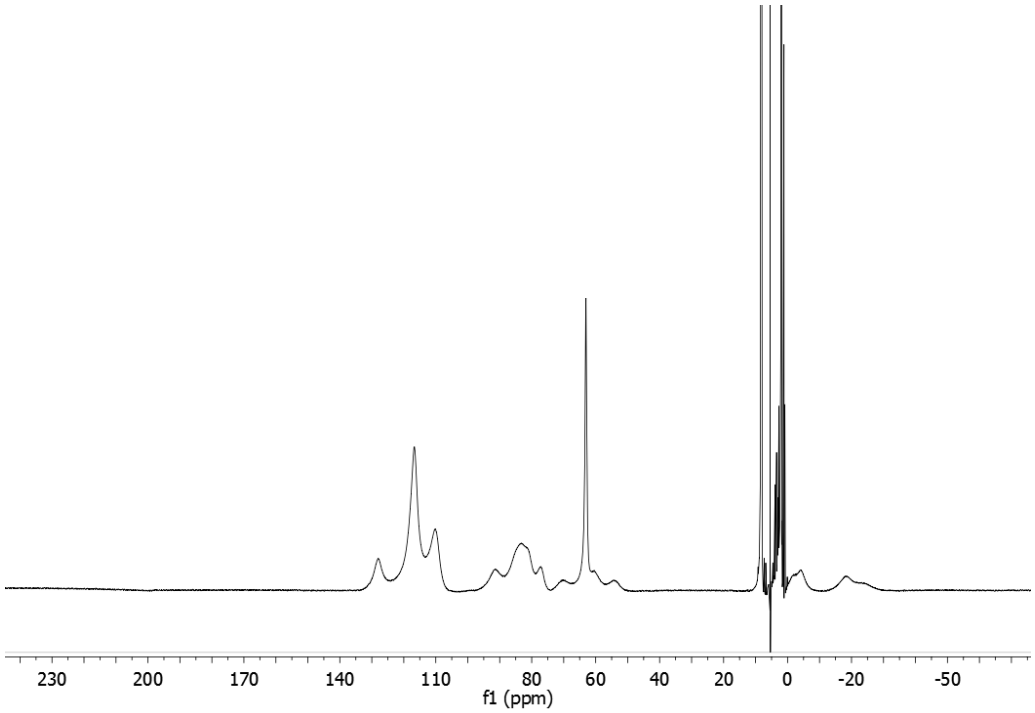

Figure S18. ^{1}H-NMR (CD_3CN, 298K) of [(MeO-PyNMe$_3$)Fe^{II}(CF_3SO_3)$_2$].

Crystal Structure Determination for [(MeO-PyNMe$_3$)Fe^{II}(CF$_3$SO$_3$)$_2$]

Crystals of $C_{18}H_{26}F_6FeN_4O_7S_2$ were grown from slow diffusion of diethyl ether in a 10:1 (v/v) dichloromethane : acetonitrile solution of the compound, and used for low temperature (100(2) K) X-ray structure determination. The measurement was carried out on a *BRUKER SMART APEX CCD* diffractometer using graphite-monochromated MK radiation (l = 0.71073 Å) from an x-Ray Tube. The measurements were made in the range 2.3 to 28.3° for θ. Full-sphere data collection was carried out with ω and φ scans. A total of 36725 reflections were collected of which 6034 [R(int) = 0.033] were unique. Programs used: data collection, Smart;[5] data reduction, Saint+;[6] absorption correction, SADABS;[7] structure solution and refinement was done using SHELXTL.[8]

The structure was solved by direct methods and refined by full-matrix least-squares methods on F^2. The non-hydrogen atoms were refined anisotropically. The H-atoms were placed in geometrically optimized positions and forced to ride on the atom to which they are attached.

Table S1. Crystal data for [(MeO-PyNMe$_3$)Fe^{II}(CF$_3$SO$_3$)$_2$].

Empirical Formula	$C_{18}H_{26}F_6FeN_4O_7S_2$	
Formula weight	632.39	
Temperature	100(2) K	
Wavelength	0,71073 Å	
Crystal system, space group	orthorombic, Pna21	
Unit cell dimensions	a = 17.9397(19) Å	$\alpha = 90^o$
	b = 10.0271(10) Å	$\beta = 123.32(2)^o$
	c = 13.5393(14) Å	$\gamma = 90^o$
Volume	2435.4(5) Å^3	
Density (calculated)	1.725 g/cm^3	
Absorption coefficient	0.884 mm^{-1}	
F(000)	1296	
Cell formula units_Z	1.725	
Crystal size	0.1 x 0.1 x 0.5 mm	
Θ range for data collection	2.3 to 28.3º	
Limiting índices	-23<=h<=23, -13<=k<=13, -17<=l<=18	
Reflections collected / unique	36725 / 6034 [R(int) = 0.033]	
Completeness to Θ	100% (Θ =28.3º)	
Refinement method	Full-matrix least-squares on F^2	
Data / restraints / parameters	4828/2/319	
Goodness-of-fit on F^2	1.105	
Final R indices [I>2σ(I)]	R_1 = 0.0252, wR2 = 0.0614	
R indices (all data)	R1 = 0.0264, wR2 = 0.0620	
Largest diff. peak and hole	0.527 and -0.843 e.Å^{-3}	

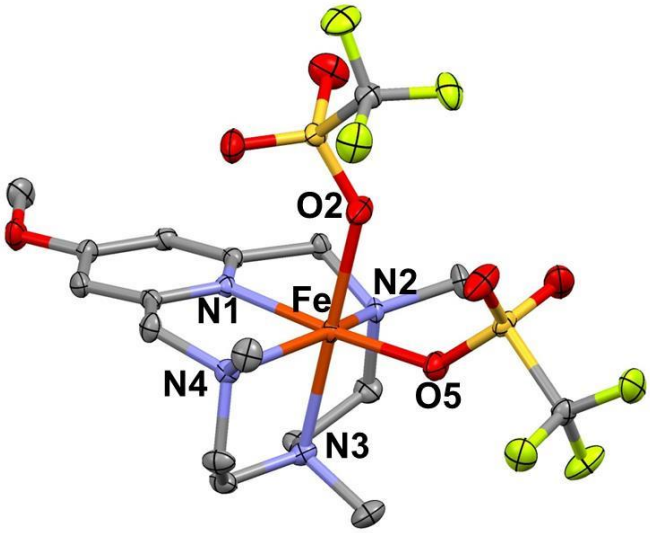

Table S2. Selected bond lengths (Å) and angles (°) for [(MeO-PyNMe$_3$)Fe^{II}(CF$_3$SO$_3$)$_2$].

Fe-N1 2.101(2)	O5-Fe-O2 83.94(8)
Fe-N2 2.266(2)	N1-Fe-N2 76.95(7)
Fe-N3 2.226(2)	N1-Fe-N3 87.72(7)
Fe-N4 2.274(2)	N1-Fe-O2 91.73(8)
Fe-O2 2.157(3)	N1-Fe-N2 76.95(7)
Fe-O5 2.068(3)	N3-Fe-N4 76.95(7)
O5-Fe-N3 96.61(8)	N3-Fe-N2 79.94(7)
O5-Fe-N2 103.47(7)	O5-Fe-N2 103.47(7)
O5-Fe-N4 104.05(7)	O2-Fe-N4 101.89(7)

II. Spectral simulations of the high-spin Fe^{III} contaminants

EPR spectra

In the present project we have struggled to find reasonable EPR and Mössbauer simulations for a variety (at least four) of high-spin (HS) Fe^{III} species observed in samples **3**(CPCA) and **2**(CPCA). The HS Fe^{III} spectral components, and their distribution, observed in **2**(CPCA) and **3**(CPCA) samples are essentially the same. We focus here on the description of the spectra of the ^{57}Fe sample used for analysis of the Mössbauer and EPR spectra (Figure 2-4 of main text) of **3b**(CPCA).

The observed HS Fe^{III} species are probably not just bothersome contaminants from side reactions as often observed in high valent oxidation chemistry. Thus, **3**(CPCA) and **2**(CPCA) were generated at -70 °C in an optical cuvette in a Unisoku cryostat under pseudo-steady state conditions; the Fe^{III} species, perhaps all of them, evidently are part of the active reaction mixture. The conditions of generating and transferring samples were optimized for sample concentrations (≈ 0.5 mM **3**(CPCA), 1 mM total Fe) suitable for a Mössbauer study. While a preparation temperature of –70 °C allowed transfer into the EPR tubes and Mössbauer cups with minimal decay of the reactive **3b**(CPCA), the solutions were very viscous; we noticed, in the late stage of our studies, that during freezing of the EPR samples void volumes can form which subsequently fill with liquid nitrogen from the storage dewar. Thawing of the liquid nitrogen inclusions during transfer of the sample to the EPR cryostat then can lead to gaps in the packing of the sample, spoiling determination of the spin concentrations.

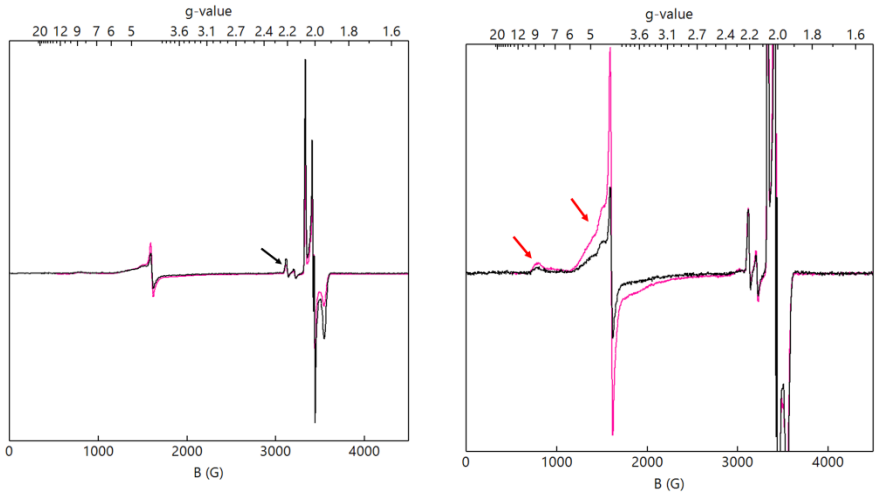

Figure S19. Wide EPR scan of the ^{57}Fe sample **3**(CPCA) at T = 15 K (sample of Figure 2; same material as Mössbauer sample of Figures 3 and 4 in the main text). Black trace: Sample recorded after 4 months of storage in liquid N_2. Species **3b**(CPCA) had 0.36 mM spin concentration which is about 30% lower than expected from analysis of the Mössbauer spectra. Inspection of the sample revealed air bubbles. Magenta trace: Sample recorded after an unsuccessful attempt to improve packing by thawing in -80 °C ethyl acetate bath and refreezing. Left panel: Spectra as recorded. Arrow points at the g = 2.20 feature. This signal has contributions from low-spin Fe^{III} species **3a**(CPCA) [Intensity 1/50 of **3b**(CPCA).] and the g_{mid} = 2.14 species (g = 2.21, 2.14, 1.97). Right panel: Spectra vertically adjusted for matching the g = 2.07 feature of **3b**(CPCA). The figure shows that all HS Fe^{III} species increase when **3b**(CPCA) decays. Left arrow point at the g_y = 8.75 resonance of the E/D = 0.16 species.

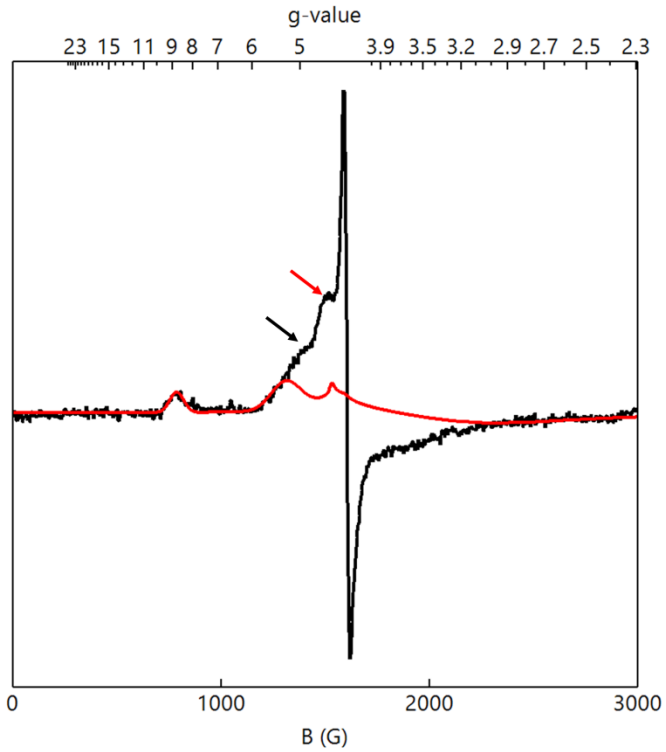

Figure S20. Low field region of black trace of Figure S19. Shown in red is a SpinCount simulation of the majority high-spin Fe^{III} species #1 with $D \approx +0.7$ cm^{-1}, $E/D = 0.16$ and $\sigma_{E/D} = 0.05$. This species represents approximately 60% of the HS Fe^{III}. The second simulated feature from the left belongs to the $g_z = 5.32$ resonance of the first excited Kramers doublet. The signals not covered by the simulations represent not more than about 40% of the HS Fe^{III} (the intrinsic transition probability is high for species with E/D values near 1/3). The sharp pronounced derivative feature at g = 4.3 represents only 2% of the Fe in the sample.

Figure S19 shows wide scan EPR spectra of a sample **3**(CPCA) recorded at T = 15 K at two different dates. The black trace shows the initial spectrum recorded after four months of storage in liquid N_2 (the delay was caused by repair of the microwave bridge). Simulation of the spectrum of Figure 2B (main text) yielded 0.30 mM spin concentration for **3b**(CPCA), which is about 30% lower than expected from analysis of the parallel Mössbauer sample. Inspection of the sample revealed air bubbles in the frozen sample. An attempt was made to improve packing by immersing the sample in an ethyl acetate bath at – 80 °C and refreezing. The magenta trace shows the spectrum recorded after refreezing. Comparison of the spectra shows that a substantial portion of species **3b**(CPCA) has decayed (as much as 30%) and that the decay lead to an increase of the signals in the g = 3.5 – 9 region where three the high-spin Fe^{III} species contribute. The majority S = 5/2 Fe^{III} species of the low field spectrum of Figure S20 (outlined by the red curve) contributes a signal at g_{eff} = 8.75, which can be assigned to a complex with D > 0 and E/D ≈ 0.16. Variable temperature studies down to T ≈ 2 K (not shown) show that this signal is associated with the electronic ground Kramers doublet. The standard S = 5/2 spin Hamiltonian

$$\boldsymbol{H} = D\left[\boldsymbol{S_z^2} - \frac{35}{4} + \frac{E}{D}\left(\boldsymbol{S_x^2} - \boldsymbol{S_y^2}\right)\right] + \beta g_0\, \boldsymbol{B}\cdot\boldsymbol{S} \qquad (1)$$

predicts for D > 0, E/D = 0.16 and g_0 = 2.00 a *ground* doublet with *effective* g-values at g_x = 2.53, g_y = 8.75, and g_z = 1.33; the *middle* doublet is predicted to have g_x = 3.26, g_z = 2.93 and g_z = 5.32. The variable temperature spectra suggest that D ≈ 0.5 - 0.7 cm^{-1}, estimated by following the g_y = 8.75 resonance down to T = 2 K. For this D value the three Kramers doublets of the ferric ion have nearly equal population at T = 15 K.

The g_y = 8.75 resonance has a width of 10 mT, indicating that at least one of the spin Hamiltonian parameters is distributed; the parameter often used and most sensitive to distributed environments is E/D. Using a Gaussian distribution for E/D with $\sigma_{E/D}$ = 0.05 and a 1 mT packet width produced simulations matching the observed width. This value of $\sigma_{E/D}$ broadens the predicted ground state resonances at g_x = 2.53 and g_z = 1.33 such that they are practically unobservable (Note: The distribution in g_y implies a corresponding distribution for the spin expectation values, which significantly broadens the associated Mössbauer lines at low magnetic fields). The red line in Figure S20 is drawn to represent 60% of the HS Fe^{III}.

A second species, #2, is indicated by a shoulder near g = 5 (black arrow in Figure S20). Eq 1 predicts for E/D ≈ 0.23 an excited doublet with g_x ≈ 4.0, g_y ≈ 3.6, g_z ≈ 4.9. Roughly, this species represents about 25% of the HS Fe^{III} (about 13% of total Fe). The ground doublet of #2 has

predicted g-values at near $g_x = 1.6$, $g_y = 9.3$ and $g_z = 1.0$. The feature at $g_y = 9.3$ would have very low intensity and would be hidden by the more intense $g_y = 8.75$ feature of the E/D = 0.16 species.

A further HS Fe^{III} signal, #3, is associated with the shoulder at $g \approx 4.5$ (red arrow in Figure S20). It is associated with the first excited state of a species with E/D = 0.295 that represents ca. 10% of the HS Fe^{III}.

Finally, the sharp derivative feature at g = 4.3 belongs to a species, #4, with E/D ≈ 1/3 that contributes roughly 2% of the HS Fe^{III} absorption.

The red line in Figure S21 is a superposition of the simulations of the four species using the parameters listed in Table S3. For these simulations D was kept fixed at 0.7 cm^{-1}.

Finally, Figure S22 compares the low field regions of the two spectra of Figure S19 such that the intensities at $g_y = 8.75$ are matched. The plot shows that all HS Fe^{III} species present initially gain intensity upon the decay of **3b**(CPCA).

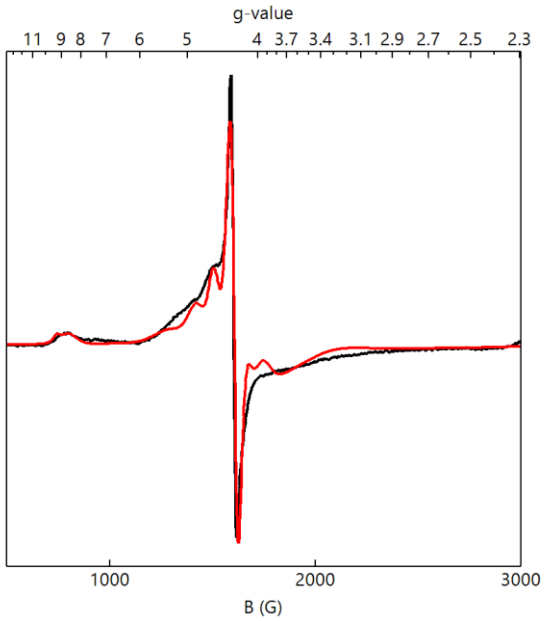

Figure S21. Spectral simulation of the four HS Fe^{III} species of the ^{57}Fe sample of Figure S19 (black curve). Parameters and proportions are listed in Table S3. The sample had trapped air bubbles and thus the spin concentrations could not be determined. The concentrations are given as % Fe^{III}. The Mössbauer analysis of the parallel sample (no air bubbles) shows that the HS Fe^{III} accounts for 42% of 1 mM Fe.

Table S3. Spin Hamiltonian parameters of species #**1 - 4** contributing to the spectral simulation of Figure S21.

Species #	**1**	**2**	**3**	**4**
g(x, y, z)	(2,2,2)	(2,2,2)	(2.03, 2.00, 2.05)	(2.01, 2.01, 2.01)
D (cm^{-1})	0.7	0.7	0.7	0.7
E/D	0.15	0.23	0.295	0.33
σ(E/D)	0.05	0.022	0.01	0.01
% of HS Fe^{III}	60	26	10	4

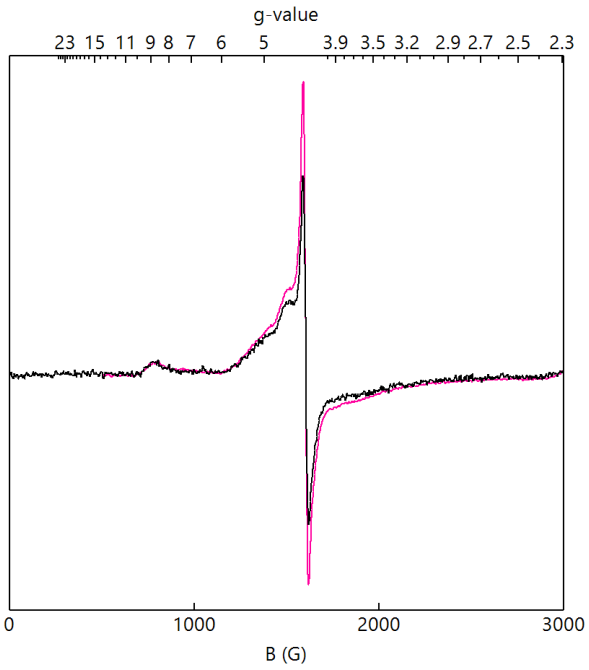

Figure S22. Low field region of the two spectra of Figure S19 after adjusting vertical scales for optimal match at g = 8.75. In our attempts to remove air bubbles, 30% of **3b**(CPCA) decayed and accumulated as additional HS Fe^{III}. This figure shows that all Fe^{III} species gained intensity nearly proportional to their initial presence. The mismatch near g = 4.3 accounts for only 2% of the Fe in the sample.

Mössbauer spectra

We describe briefly the procedure to simulate the 2.0, 4.0 and 7.0 T spectra of the S = 5/2 species shown in Figure 3 and 4 of the main text. At 4.2 K and for B = 7.0 T only the electronic ground level is significantly (≈ 90%) populated for D ≈ +0.7 cm^{-1}. The ground state is the M_S = -5/2 level. The magnetic splitting of the 7.0 T Mössbauer spectrum is determined by the effective field $\mathbf{B}_{eff} = \mathbf{B}_{int} + \mathbf{B}$, where $\mathbf{B}_{int} = -\langle\mathbf{S}\rangle\cdot\mathbf{A}/g_n\beta_n$ and $\langle\mathbf{S}\rangle$ is the expectation value of the electronic spin. For D = +0.7 cm^{-1}, $\langle S_{x, y, z}\rangle \approx$ -2.5 (to within 1%) at B = 7.0 T. As the electronic Zeeman splitting dominates, the components of $\langle\mathbf{S}\rangle$ are independent of D and E/D. At B = 7.0 T the M_S = -3/2 state is populated by ≈ 10% and its spectral signature has been identified in the main text. Because the quadrupole splittings of the Fe^{III} species are small, the 4.2 K high field Mössbauer spectramostly determined by **A**. The spin Hamiltonian parameters listed in Table S4 work quite well for B = 2.0, 4.0 and 7.0 T. One site corresponds to the E/D = 0.16 majority species indicated by EPR. For the Mössbauer simulations we assumed that this site 1 represents 30% of the Fe in the sample. The E/D ≈ 0.23 species was assumed to represent 12% of Fe. We believe that the differences in the A-tensors (A_{iso} = -19.3 T *vs* -21.1 T) are real but the listed anisotropies of A-tensors are probably not meaningful. The reader should take these parameters in the spirit of an effort to come to grips with the contaminants. Site #3 and #4 are somehow absorbed in the two species of Table S4. That this works is not surprising since the values of E/D and D do not matter in strong applied fields for small D The Mössbauer simulations sort the Fe^{III} species according to their A-values.

We have not been able to properly link the listed parameters with particular the HS Fe^{III} features observed in B = 45 mT applied fields. This should not come as a surprise, for various reasons: (i) our EPR analysis, while not as quantitative as one may wish, indicates that at least four HS Fe^{III} species are present. At 4.2 K the contribution of the HS Fe^{III} is distributed among 4×3 = 12 Kramers doublets; (ii) the B = 45 mT spectra depend on four sets of D, E/D, ΔE_Q, η values in addition to the four A-tensors; (iii) the major species has a significant $\sigma_{E/D}$ which broadens the Mössbauer absorption lines; (iv) there is no evidence that the EPR spectra of **3b**(CPCA) and **2b**(PAA) suffer from spin-dipolar broadening caused by partial aggregation. This is not necessarily true for the HS Fe^{III} species which have larger magnetic moments. Weak spin dipolar broadening might affect the EPR spectra by broadening that is not easily recognized. Similarly,

weak spin-dipolar interactions would be difficult to recognize in the 45 mT Mössbauer spectra; in strong applied fields these interactions would be decoupled; (v) there is another good reason for avoiding the B = 0.45 T Mössbauer spectra for preparing the spectrum of **3**(CPCA). At 4.2 K the middle Kramer's doublets of the HS Fe^{III} species are substantially populated for $D \approx 0.7$ cm^{-1}. Their associated Mössbauer absorption is entirely in the velocity range of **3**(CPCA). In strong applied fields the middle Kramers doublets are essentially depopulated at 4.2 K, and thus the spectral range crucial for identifying **3b**(CPCA) is kept reasonably clean from contaminants.

Table S4. S = 5/2 spin Hamiltonian parameters used to simulate the HS Fe^{III} species.[a]

Species	E/D = 0.16 species	E/D = 0.23 species
D (cm^{-1})	0.7	0.7
E/D	0.16	0.23
ΔE_Q (mm/s)	-0.8	0.76
η	1	-2.2
$A_x/g_n\beta_n$ (T)	-19.5	-20.9
$A_y/g_n\beta_n$ (T)	-19.2	-20.6
$A_z/g_n\beta_n$ (T)	-19.2	-21.6
δ (mm/s)	0.43	0.44
Percentage of total Fe	30%	12%

[a] The B = 2.0, 4.0 and 2.0 T Mössbauer spectra are insensitive to E/D and D (for $D < 1$ cm^{-1}) and only moderately sensitive to ΔE_Q and η.

III. EPR and Mössbauer spectra of $[(PyNMe_3)Fe^{V}(O)(OC(O)cy)]^{2+}$ (2b(CPCA))

Due to many contaminating species in our previous preparations we were not able to identify the Mössbauer spectrum of **2b**.[9] During the past year we improved our preparations, primarily by using as oxidant cyclohexane peroxycarboxylic acid rather than peracetic acid as oxidant, yielding a g_{max} = 2.07 species designated in the main text as **2b**(CPCA). Use of this oxidant eliminated the impurities in the g = 2 region. Briefly, the parameters of **2b**(CPCA) are within the "uncertainties" the same as those of **3b**(CPCA). These "uncertainties" arise because one has to simulate the spectra of largely unknown species and estimate what fraction of the absorption they represent. Preparations of **2b**(CPCA) had ca. 26% of identifiable Fe^{III} (mainly a species with E/D ≈ 0.19). There is perhaps another 15% high-spin ferric material, possibly in partially aggregated form, indicated by the broad and unaccounted features near –4 mm/s and +4 mm/s Doppler velocity in the 7.0 T spectrum of Figure 3 in the main text. However, the samples have a contribution of low-spin Fe^{III} peroxo complex **3a**(CPCA) (g_{max} = 2.20). As for **2a**(PAA) and **2b**(PAA) the EPR and UV-vis spectra of **2a**(CPCA) and **2b**(CPCA) indicate that the two species are in fast equilibrium in solution. The Mössbauer spectrum of **2a**(CPCA) is completely buried under the absorption of **2b**(CPCA). However, from an EPR analysis (Figure S23) we found that that [**2b**(CPCA)]:[**2a**(CPCA)] = 7:1, and that **2a**(CPCA) has g-values, g = (2.20. 2.19, 1.99), which fit well to the Griffith model for low-spin Fe^{III} species,[10] a happy circumstance which can be used to calculate the ^{57}Fe A-tensor. As the Griffith model worked very well for the recently studied S = 1/2 (TPA)Fe^{III}-acylperoxo complex,[11] we have used it to simulate **2a**(CPCA). We also found, by comparing different preparations, that our sample contained an S = 0 diferric species (roughly 5%). It is possible that the sample, like the sample of **3b**(CPCA), contained a small percentage (≈5%) of a $[(PyNMe_3)Fe^{IV}(O)(NCMe)]^{2+}$ (**4**) contaminant. After subtracting the simulated spectra of the contaminants we arrived at a spectral representation of **2b**(CPCA) (see caption of Figure S24). The simulations for **2b**(CPCA) are shown in magenta. The parameters obtained for **2b**(CPCA), listed in Table 1 of the main text, are close to those obtained for **3b**(CPCA), perhaps the same within the uncertainties. (We analyzed the **2b**(CPCA) data before we recognized by ongoing EPR studies that the MeO- substituent would yield samples of higher spectral purity).

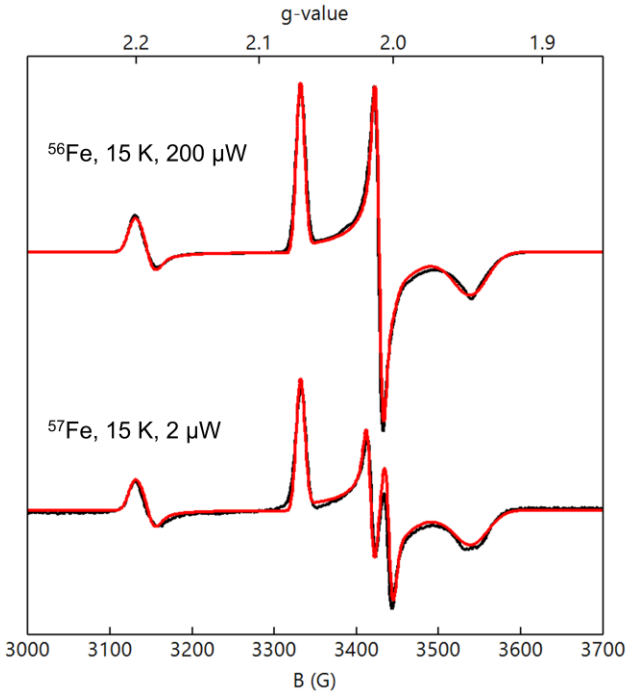

Figure S23. g = 2 region of EPR spectra of $[(PyNMe_3)Fe^{V}(O)(OC(O)cy)]^{2+}$, **2b**(CPCA), and $[(PyNMe_3)Fe^{III}(\kappa^2\text{-}OC(O)cy)]^{2+}$, **2a**(CPCA). Black: experimental spectra; red: simulations. Top: Sample containing 1 mM Fe in natural abundance (2% ^{57}Fe). The majority species **2b**(CPCA) (g = 2.01, 2.07 and 1.94) and minority species **2a**(CPCA) (g = 2.20, 2.19, 1.99) were simulated in the concentration ratio 7:1. Spin concentrations by SpinCount simulations were: 0.43 mM **2b**(CPCA) and 0.06 mM **2a**(CPCA). Bottom: ^{57}Fe-enriched (95%) sample. g_{mid} = g_x of **2b**(CPCA) is split into a doublet by a large A_x = 62 MHz. For the simulations the principal axis systems of the g- tensor and the ^{57}A-tensor were kept collinear. The hyperfine splittings at g = 2.07 and 1.94 are smaller than 10 MHz. Spin concentrations: ≈ 0.52 mM **2b**(CPCA) and ≈ 0.07 mM **2a**(CPCA).

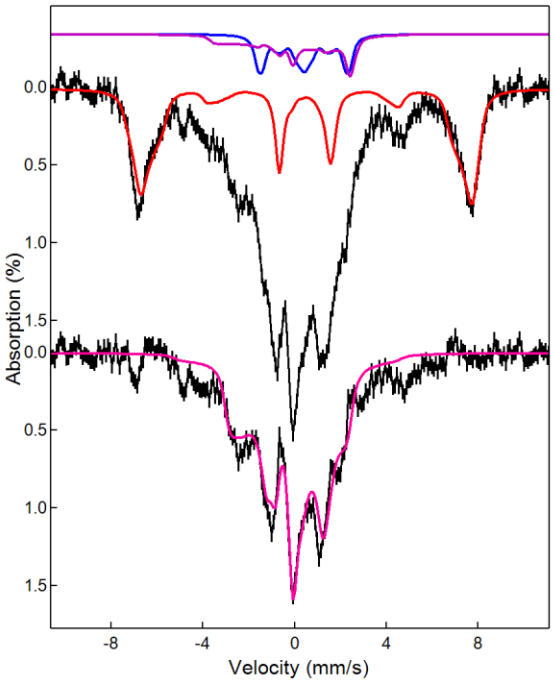

Figure S24. 4.2 K/7.0T spectra of **2b**(CPCA) sample**.** Top: Raw data. The solid lines are spectral simulations approximating a series of spectral impurities. Red: high-spin Fe^{III}; drawn to represent 30% of Fe; Magenta: S = ½ species **2a**(CPCA); 7% of Fe; g = (2.20, 2.19, 1.99), $A_{x,y.z}$ = (+6.8, +8.6, -71.7) MHz from the Griffith model,[11] and ΔE_Q = -1.6 mm/s, η = 0, δ = 0.17 mm/s (Note: these are not experimentally determined parameters; they are an educated guess to account for **2a**(CPCA)). Blue: S = 0 diferric species, 5% of Fe, ΔE_Q = +2.0 mm/s and δ = 0.40 mm/s spectrum and η = 1 (estimated). Bottom: Spectrum of **2b**(CPCA) obtained after subtracting the contaminants. Magenta curve represents 48% of Fe; the true amount of **2b**(CPCA) is estimated to be between 45% and 50%.

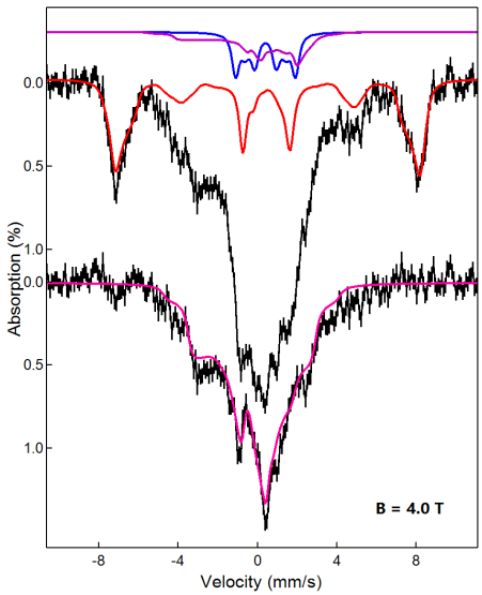

Figure S25. 4.2K/4.0 T spectrum of **2b**(CPCA). Top: Raw data. Solid lines are simulations of contaminants. Bottom: Spectrum of **2b**(CPCA) sample obtained after subtracting simulations of contaminants. Magenta curve is drawn to represent 48% Fe^{V} of the Fe in the sample.

IV. Mössbauer spectra of $[(PyNMe_3)Fe^{IV}(O)(NCMe)]^{2+}$ (4)

A sample containing **4** was obtained by treating 1 mM $[(PyNMe_3)Fe^{II}(CF_3SO_3)_2]$ (**1**) in 3:1 acetone:acetonitrile (v/v) with 4 equivalents of 2-^{t}BuSO$_2$-C$_6$H$_4$IO (sArIO) at -40 °C. We have not yet found a procedure to generate **4** in high yield. The zero field Mössbauer spectrum shown in Figure S26A exhibits a quadrupole doublet with $\Delta E_Q = 0.30 \pm 0.02$ mm/s and $\delta = 0.05 \pm 0.01$ mm/s; this doublet, assigned to **4**, accounts for ≈ 40% of the iron in the sample. The observation of a doublet for B = 0 indicates a complex with integer electronic spin. The broad features are contaminants. One contaminant, accounting for ≈ 43% of the iron in the sample, belongs to one or more high-spin Fe^{III} species. The remainder (≈ 15% of Fe), absorbing between - 4 mm/s and + 3 mm/s, is a paramagnetic component of unidentified nature.

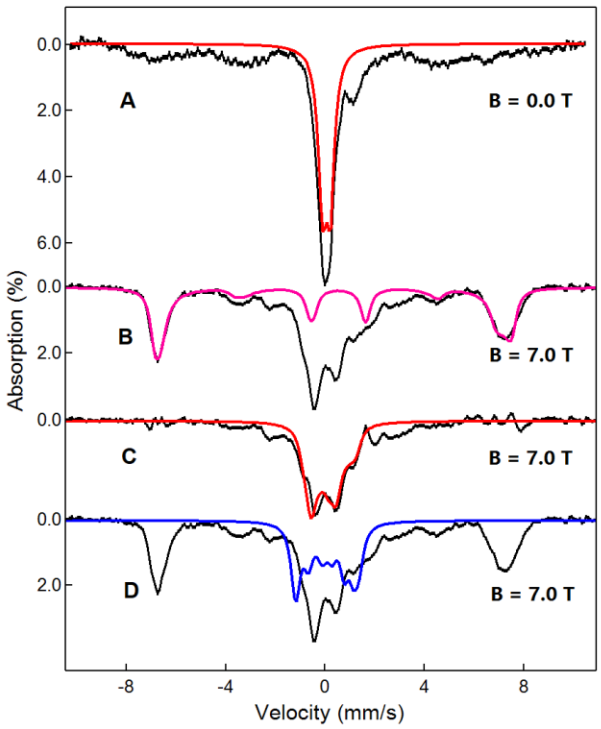

Figure S26. 4.2 K Mössbauer spectra of 0.8 mM $[(PyNMe_3)Fe^{II}(CF_3SO_3)_2]$ (**1**) in MeCN treated with a 4-fold excess of sArIO. (A) The spectrum outlined in the zero field spectrum by the red line is assigned to $[(PyNMe_3)Fe^{IV}(O)(NCMe)]^{2+}$ (**4**); this species represents ≈ 40% of the Fe in the sample. (B) Spectrum recorded for B = 7.0 T. The magenta line is a spectral simulation approximating the S = 5/2 contaminant (roughly 43%; perhaps more than one species). (C) B = 7.0 T spectrum obtained after subtracting the S = 5/2 contaminant. The red line is a simulation

for **4**, assuming that this species has parameters typical of those observed for S = 1 Fe^{IV}=O complexes, namely D = 27 cm^{-1}, E/D = 0, A_x = A_y = -29 MHz, A_z = -7 MHz, η = 0, ΔE_Q = 0.30 mm/s and δ = 0.05 mm/s; ΔE_Q and δ were obtained from the zero field spectrum of (A). (D) The blue line assumes D = 15 cm^{-1}, rather than D = 27 cm^{-1}, for the simulation of the Fe^{IV}=O species. This choice for D produces an unacceptable large magnetic splitting (showing that βB/D is chosen too large).

The following spin Hamiltonian was used for the spectral simulations:

$$\boldsymbol{H} = D\left[\boldsymbol{S}_z^2 - 2 + \frac{E}{D}\left(\boldsymbol{S}_x^2 - \boldsymbol{S}_y^2\right)\right] + \beta \boldsymbol{B} \cdot \widetilde{g_0} \cdot \boldsymbol{S} + \boldsymbol{S} \cdot \widetilde{\boldsymbol{A}} \cdot \boldsymbol{I} + \boldsymbol{H_Q} - g_n \beta_n \boldsymbol{B} \cdot \boldsymbol{I}$$

Figure S26 B-D show a 7.0 T spectrum of **4**. We have also recorded spectra for B = 2.0 and 4.0 T (not shown). The solid red line is an S = 1 spin Hamiltonian simulation using parameters typically encountered for S = 1 Fe^{IV}=O species. The blue line represents a simulation assuming D = 15 cm^{-1}; this D-value is clearly too small as it produces a magnetic splitting that is too large (Roughly, the magnetic splitting is proportional to A_x (βB/D). The really important parameter for the present study is δ = 0.05(2) mm/s, which is significantly larger than δ = -0.06 mm/s and δ = -0.08 mm/s obtained for **2b**(CPCA) and **3b**(CPCA), respectively.

Above we have tacitly assumed that MeCN is coordinated to the Fe^{IV}=O. This assumption is not unreasonable as this solvent is found to coordinate to a variety of Fe^{IV}=O species. A geometry-optimized DFT structure of the *trans* isomer of $[(MeO\text{-}PyNMe_3)Fe^{IV}(O)(NCMe)]^{2+}$ (oxo ligand *trans* to the pyridine) is shown in Figure S27. The DFT value for the isomer shift, δ = 0.05 mm/s, is in good agreement with the experimental values. The DFT values for the Fe=O bond length and $\nu_{Fe=O}$ are 1.67 Å and 842 cm^{-1}, respectively.

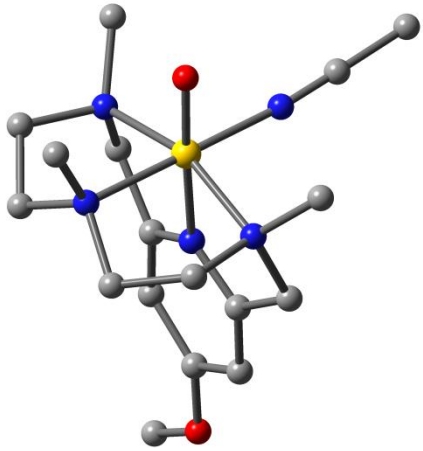

Figure S27. Optimized BP86/6-311G DFT structure of the *trans* isomer of [(MeO-PyNMe$_3$)Fe^{IV}(O)(NCMe)]$^{2+}$. Calculated bond lengths are: Fe-O$_{oxo}$ = 1.67 Å, Fe-N$_{py}$ = 1.98 Å, Fe-NCMe = 1.95 Å, average of the other three (Fe-N) bonds = 2.08 Å. This figure is also pertinent for [(MeO-PyNMe$_3$)Fe^{V}(O)(NCMe)]$^{3+}$, with the following bond lengths: Fe-O$_{oxo}$ = 1.62 Å, Fe-N$_{py}$ = 1.96 Å, Fe-NCMe = 2.00 Å.

V. Molecular Orbital of the *trans* isomer of 3b(CPCA) involving Fe, O1 and O2

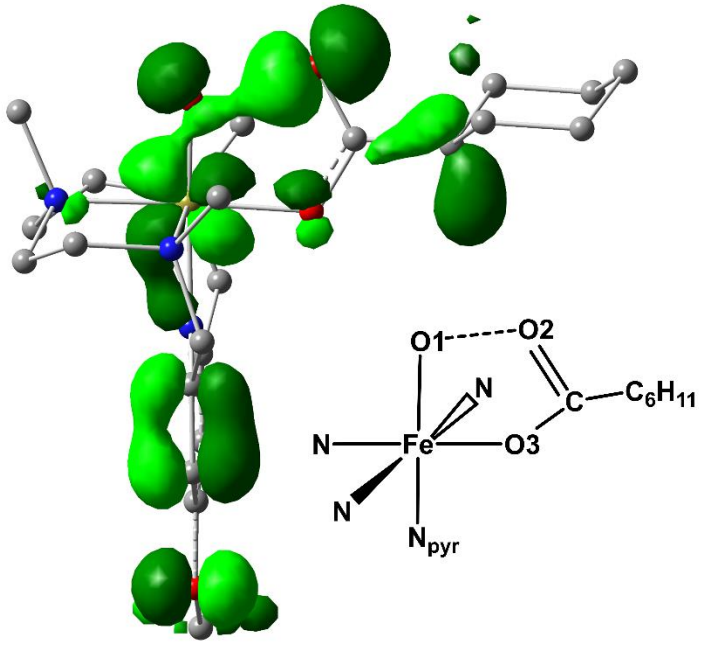

Figure S28. Contour plot of orbital#121 in α-space the *trans* isomer of **3b**(CPCA) (isovalue = 0.04), showing three-center bonding involving 2p orbitals of O1 and O2 and $3d_{xz}$ from Fe.

VI. α-HOMO and spin density of the *cis* isomer of 3b(CPCA)

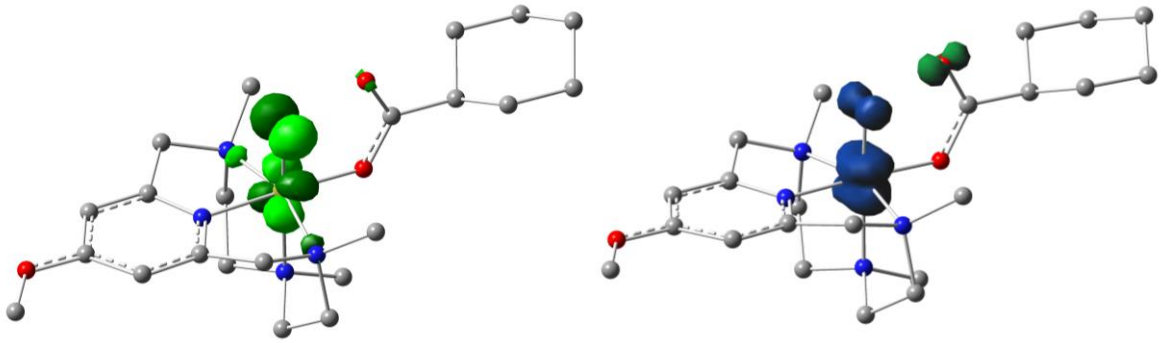

Figure S29. α-HOMO (left) and spin density (right) of the *cis* isomer of **3b**(CPCA) (Isovalue of MO = 0.10, Isovalue of spin density = 0.02).

VII. Comparison of selected parameters for the *cis* and *trans* isomers of 3b(CPCA) and 2b(CPCA) obtained from DFT

Table S5. Comparison of selected parameters for *trans* and *cis* isomers of species **2b**(CPCA) and **3b**(CPCA) obtained from DFT. Parameters were calculated using the BP86/6-311G functional/basis set. The *trans* isomer was found to be 0.3 kcal/mol lower in energy than the *cis* isomer for species **2b**(CPCA) and **3b**(CPCA).

Configuration	*trans*[a]		*cis*	
Species	**3b**(CPCA)	**2b**(CPCA)	**3b**(CPCA)	**2b**(CPCA)
Substituent	MeO	H	MeO	H
O1-O2 (Å)	2.04	2.04	2.01	2.01
Fe-O1 (Å)	1.65	1.65	1.65	1.65
ν(Fe-O1) (cm^{-1})	837	836	815	815
δ(mm/s)	-0.02	-0.01	-0.02	-0.02
ΔE_Q (mm/s)	0.77	0.83	1.58	1.55
η	0.26	0.24	0.58	0.64
A_{SD} (MHz)	-26.8, +5.6, +21.2	-26.8, +5.6, +21.2	-27.2, +4.7, +22.5	-28.0, +6.0, +22.0,
g_x, g_y, g_z	2.02, 2.04, 1.98	2.02, 2.04, 1.98	2.02, 2.04, 1.98	2.02, 2.04, 1.98

[a] Oxo group O1 *trans* to the pyridine nitrogen

VIII. DFT of a hypothetical $[(MeO\text{-}PyNMe_3)Fe^{V}(O)]^{3+}$ complex

In the course of our DFT studies of **2b**(PAA), **2b**(CPCA) and **3b**(CPCA), we rotated the carboxylate ligand around the Fe–O3 bond to increase the O1–O2 distance beyond the optimized 2.04 Å distance, in order to determine if this change would yield an electronic structure with increased Fe^{V} character. In a series of relaxed scans in which the O1–O2 distance was fixed at 2.20, 2.80, or 3.00 Å, we noted that the complex acquired increasing $[(MeO\text{-}PyNMe_3)Fe^{IV}(O)(^{\bullet}OC(O)R)]^{2+}$ character, as indicated by an increase in the negative spin density at O2 and an increase in the value of $\langle\psi_{BP86}|S^2|\psi_{BP86}\rangle$. We then optimized, mainly for curiosity, a complex for which the carboxylate bound at O3 had been removed, to give the Fe^{V}=O structure shown in Figure S30. For this S = ½ complex an ORCA calculation returned g-values at 2.03, 2.01 and 1.97. The expectation value $\langle\psi_{BP86}|S^2|\psi_{BP86}\rangle$ = 0.76 is identical to that obtained for $[(TAML)Fe^{V}(O)]^{-}$, see Table 3 of the main text. The isomer shift is quite low at δ = -0.34 mm/s, and the calculated Fe–O bond length is 1.58 Å, which compares with the 1.60 Å value calculated for the TAML complex. An interesting feature of the 5-coordinate $[(MeO\text{-}PyNMe_3)Fe^{V}(O)]^{3+}$ complex is the high vibrational frequency ν(Fe–O1) = 994 cm^{-1}, which is about 120 cm^{-1} higher than that calculated (and observed) for $[(TAML)Fe^{V}(O)]^{-}$.

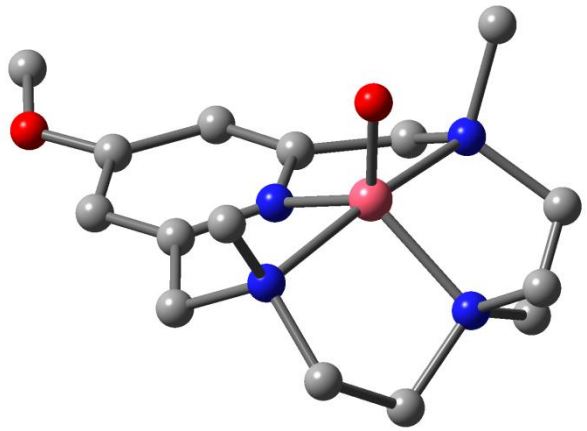

Figure S30 Optimized structure of $[(MeO\text{-}PyNMe_3)Fe^{V}(O)]^{3+}$ using BP86/6-311G.

IX. Fe^{V}=O bond length in a hypothetical 6-coordinate $[(TAML)Fe^{V}(O)(NCMe)]^{-}$ complex

$[(TAML)Fe^{V}(O)]^{-}$ is a 5-coordinate complex with experimental parameters indicating a pure S = ½ configuration. An EXAFS study showed an Fe=O bond length of 1.58 Å and B3LYP/6-311G DFT calculations yielded 1.60 Å.[12] These results raised the question as to whether the EXAFS Fe–O bond length for **2b**(CPCA), 1.63 Å, is too long for an Fe^{V} complex. To study this question we considered a hypothetical 6-coordinate TAML complex by adding, *in silico*, an acetonitrile ligand *trans* to the oxo group. In $[(TAML)Fe^{V}(O)]^{-}$ the Fe atom is 0.42 Å above the plane defined by the four amido nitrogen atoms. For the BP86/6-311g calculations of the 6-coordinate complex the Fe-N_{NCMe} distance was fixed to values ranging from 1.86 Å to 2.06 Å in steps of 0.02 Å and the eleven resulting FeO-constrained structures were optimized. These calculations yielded the Fe=O bond lengths represented by the red full circles in Figure S31. The blue circle represents the 5-coordinated TAML complex (Fe–NCMe = ∞) and is on the line defined by the red dots. In the *in silico* $[(MeO\text{-}PyNMe_3)Fe^{V}(O)(NCMe)]^{3+}$ the Fe-N_{NCMe} bond length is 2.00 Å. At this Fe-N_{NCMe} distance the 6-coordinate TAML complex has a calculated Fe-O = 1.64 Å, suggesting that the experimental 1.63 Å obtained for **3b**(CPCA) is consistent with the assignment to a 6-coordinate Fe^{V} species.

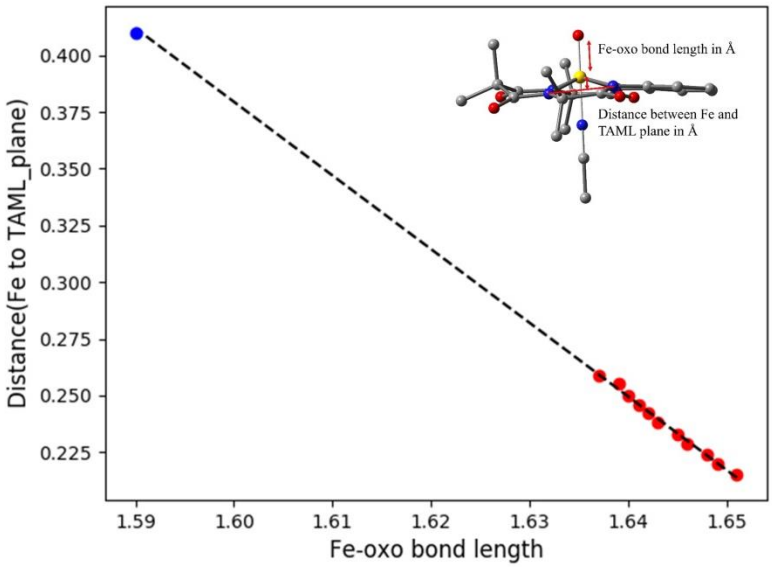

Figure S31. Plot of the out-of-plane distance of the iron *vs* Fe–oxo bond length calculated by optimizing the geometry of $[Fe^{V}(O)(NCMe)(TAML)]^{-}$ at fixed $Fe–N_{NCMe}$ distances showing a linear relationship. (Blue dot: data point for the (Fe–NCMe = ∞) 5-coordinate structure; red dots: data points for optimized structures with fixed axial $Fe–N_{NCMe}$ bonds *trans* to the oxo; black dotted line: linear fitting of red dots)

X. Resonance Raman spectra

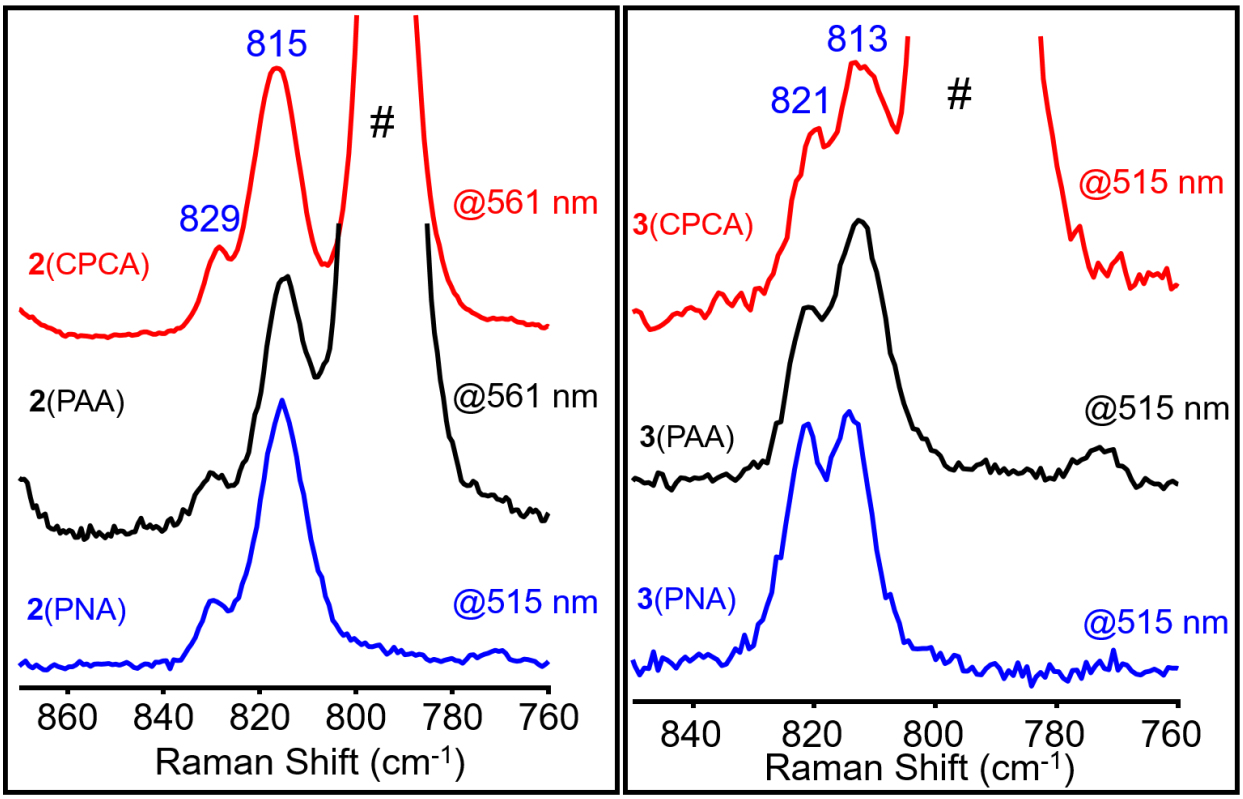

Figure S32. Resonance Raman spectra of (left) **2**(CPCA) (red), **2**(PAA) (black) and **2**(PNA) (blue) and (right) **3**(CPCA) (red), **3**(PAA) (black) and **3**(PNA) (blue). **2**(PAA), **2**(CPCA) and **3**(CPCA) were obtained in CH_3CN/acetone (1:3) and **2**(PNA), **3**(PNA) and **3**(PAA) were obtained in CH_3CN/d_6-acetone (1:3) at 77 K. Excitation wavelengths are indicated to the right of each trace. # designates an acetone solvent band.

XI. X-ray Absorption Spectroscopy (XAS)

XAS experimental section

Three XAS samples were studied, namely $[(PyNMe_3)Fe^{II}](CF_3SO_3)_2$ (**1**), **2b**(CPCA), and decayed **2b**(CPCA). The sample of **1** was prepared by dissolving this compound in acetonitrile/acetone (1:3) at 20 °C to obtain a 10 mM solution, which was then transferred to a XAS cup and frozen in liquid nitrogen. The XAS sample for **2b**(CPCA) was prepared by reacting 2 mM **1** in an acetonitrile/acetone (1:3) solution with 10 equiv. CPCA at -70 °C, which was then transferred to a XAS cup and frozen in liquid nitrogen for XAS data collection. After XAS data collection the sample was brought to room temperature and allowed to stand for 10 min to allow **2b**(CPCA) to decay. This sample, called decayed **2b**(CPCA), was then frozen in liquid nitrogen for further XAS data collection.

Iron K-edge X-ray absorption spectra for **2b**(CPCA), decayed **2b**(CPCA), and **1** in acetonitrile/acetone (1:3) were collected on SSRL beam line 9-3 using a 100-element solid state Ge detector (Canberra) with a SPEAR storage ring current of ~500 mA at a power of 3.0 GeV. The incoming X-rays were unfocused using a Si(220) double crystal monochromator, which was detuned to 40% of the maximal flux to attenuate harmonic X-rays. Six, five and six scans of the fluorescence excitation spectra for **2b**(CPCA), decayed **2b**(CPCA), and **1** in acetonitrile/acetone (1:3), respectively, were collected from 6882 eV to 8000 eV at a temperature (10 K), which was controlled by an Oxford Instruments CF1208 continuous flow liquid helium cryostat. An iron foil was placed in the beam pathway prior to the ionization chamber I_0 and scanned concomitantly for an energy calibration, with the first inflection point of the edge assigned to 7112.0 eV. A 3-μm Mn filter and a Soller slit were used to increase the signal-to-noise ratio of the spectra.

The detector channels from the scans were examined, calibrated, averaged, and processed for EXAFS analysis using EXAFSPAK[14] to extract $\chi(k)$. Theoretical phase and amplitude parameters for a given absorber-scatterer pair were calculated using FEFF 8.40[15] and were utilized by the "opt" program of the EXAFSPAK package during curve fitting. Parameters for **2b**(CPCA), decayed **2b**(CPCA), and **1** were calculated using a model based on the available crystal structure of **1**.[9] In all analyses, the coordination number of a given shell was a fixed parameters and was varied iteratively in integer steps, while the bond lengths (R) and mean-

square deviation (σ^2) were allowed to freely float. The amplitude reduction factor S_0 was fixed at 0.9, while the edge-shift parameter E_0 was allowed to float as a single value for all shells. In any given fit, the number of floating parameters was typically equal to (2 x number of shells) + 1. The *k* range of the data is 2 – 13 $Å^{-1}$, 2 - 15 $Å^{-1}$and 2 - 14 $Å^{-1}$.

The pre-edge analysis was performed on data normalized in the "process" program of the EXAFSPAK package, and pre-edge features were fit between 7108 eV to 7118 eV using the *Fityk*[16] program with pseudo-Voigt functions composed of 50:50 Gaussian/Lorentzian functions.

X-ray Absorption Spectroscopic analysis

The XAS analysis results of **1**, **2b**(CPCA) and decayed **2b**(CPCA) in acetonitrile/acetone (1:3) are summarized in Table S6. Detailed analysis on the three complexes is given below.

Table S6. XAS analyses of **1**, **2b**(CPCA) and decayed **2b**(CPCA).

	K-edge (eV)	Pre-edge (eV)	Pre-edge area	EXAFS analysis		
				N path	r (Å)	σ^2 (x10^{-3})
1	7123.1	7112.8	4.9 units	3 N/O	1.90	4.8
				3 N/O	2.05	5.4
				6 C	2.85	2.8
				4 C	3.14	2.6
2b(CPCA)	7124.8	7114.4	15.6 units	0.5 N/O	1.63	1.4
				3 N/O	1.99	4.5
				2 N/O	2.17	6.2
				4 C	2.86	3.4
				4 C	3.00	3.5
decayed **2b**(CPCA)	7124.8	7114.3	14.3 units	3 N/O	2.02	5.3
				3 N/O	2.19	6.5
				6 C	2.97	8.5

XAS analysis of 2b(CPCA)

The Fe K-edge for a sample containing ≈ 50% **2b**(CPCA), by Mössbauer analysis, in acetonitrile/acetone (1:3) solution is observed at 7124.8 eV with a pre-edge feature arising from 1s → 3d transitions[13] at 7114.4 eV with an area of 15.6 units (Figure S33b). The Fourier transformed EXAFS data shows two prominent features at R + Δ ~ 1.4 and 2.4 and Å (see Figure 6 in the main text). The best fit reveals 0.5 O scatterers at 1.63 Å, 3 N/O scatterers at 1.99 Å and 2 N/O scatterers at 2.17 Å for the first shell and 4 C scatterers at 2.86 and 3.00 Å for the outer shell. The 0.5 O scatterer at 1.63 Å supports the presence of an Fe=O unit in **2b**(CPCA).

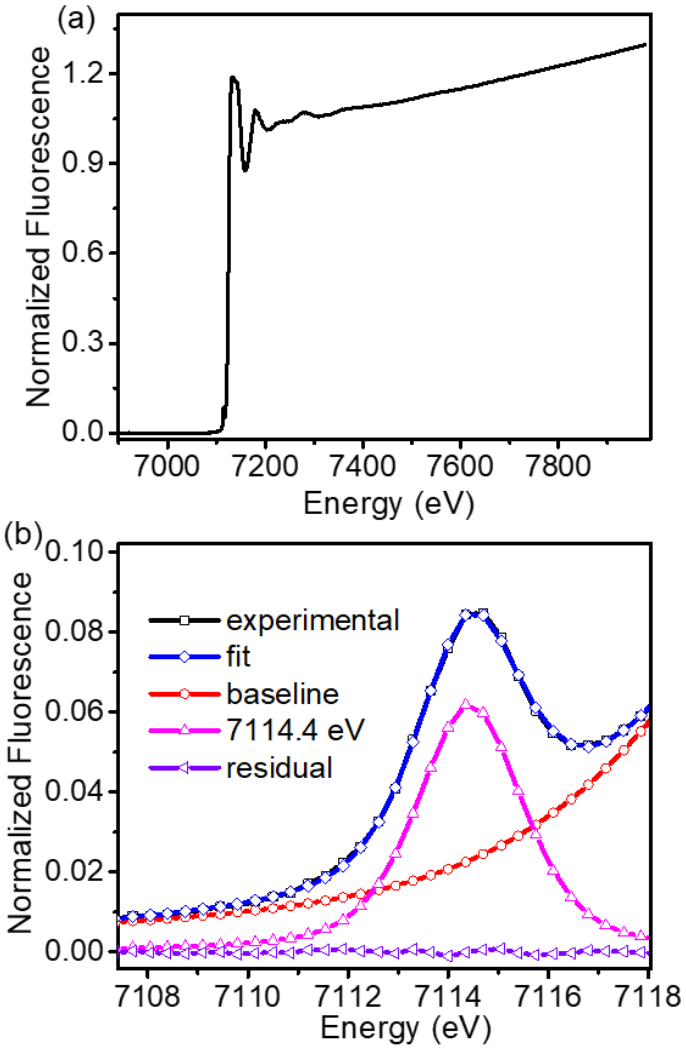

Figure S33. XAS data (top) and pre-edge analysis (bottom) of a sample containing 50% **2b**(CPCA) in acetonitrile/acetone (1:3) at 10 K.

Table S7. EXAFS fit parameters for a sample containing 50% **2b**(CPCA) in acetonitrile/acetone (1:3). Fourier transformed range k = 2-13 Å^{-1}, resolution 0.14 Å.

	Fe–N/O			Fe–N/O			Fe–O			Fe···C			GOF		
Fit	N	r (Å)	σ^2 x 10^{-3}	N	r (Å)	σ^2 x 10^{-3}	N	r (Å)	σ^2 x 10^{-3}	N	r (Å)	σ^2 x 10^{-3}	F	F’	E_0
1	6	1.98	12										358	763	-13.6
2	5	1.97	9.1										337	741	-16
3	4	1.96	6.7										320	722	-17.9
4	4	1.99	5.5	1	2.18	0							285	682	-8.9
5	3	1.98	3	2	2.16	3.5							278	674	-6.8
6	3	1.98	5.2	2	2.15	5.2	1	1.63	7				244	627	-4.2
7	3	1.99	4.5	2	2.16	6.6	0.5	1.62	1.6				225	601	-4.6
8	3	1.99	4.5	2	2.18	6	0.5	1.62	1.4	6	2.93	8.5	123	447	-2.6
9	3	2	4.5	2	2.18	5.9	0.5	1.62	1.4	4	2.93	5.9	134	468	-2.5
10	**3**	**1.99**	**4.5**	**2**	**2.17**	**6.2**	**0.5**	**1.63**	**1.4**	**4**	**2.86**	**3.4**	**117**	**438**	**-2.9**
										4	**3.00**	**3.5**			
11	3	1.99	3.2	2	2.17	3.6				4	2.86	5.9	193	562	-4.4
										4	2.98	6.7			

Scale Factor S_0^2 = 0.9. GOF = Goodness-of-fit calculated as

$$F = \sqrt{\sum k^6 \left(\chi_{\exp} - \chi_{calc}\right)^2}$$

$$F' = \sqrt{\sum k^6 \left(\chi_{\exp} - \chi_{calc}\right)^2 / \sum k^6 \chi_{\exp}{}^2}$$

XAS analysis of decayed 2b(CPCA) species

The Fe K-edge for decayed **2b**(CPCA) is observed at 7124.8 eV. There is a pre-edge feature at 7114.3 eV with a pre-edge area of 14.3 units (Figure S34). Surprisingly, the edge energy and pre-edge area of decayed **2b**(CPCA) are comparable to those of a sample containing 50% **2b**(CPCA). The EXAFS data of decayed **2b**(CPCA) (Figure S35) shows two prominent features at R + Δ ~ 1.4 and 2.4 Å. Best fits reveal 3 shorter N/O scatterers at 2.02 Å and 3 longer N/O scatterers at 2.19 Å (Table S8), distances typical for metal-ligand bonds of a high-spin Fe^{III}. In the secondary coordination sphere there are 6 C scatterers at 2.97 Å, and 4 C scatterers at 3.14 Å arising from the $PyNMe_3$ ligand. More importantly the EXAFS analysis of decayed **2b**(CPCA) did not require a scatterer at 1.63 Å, indicating the absence of a terminal Fe=O bond.

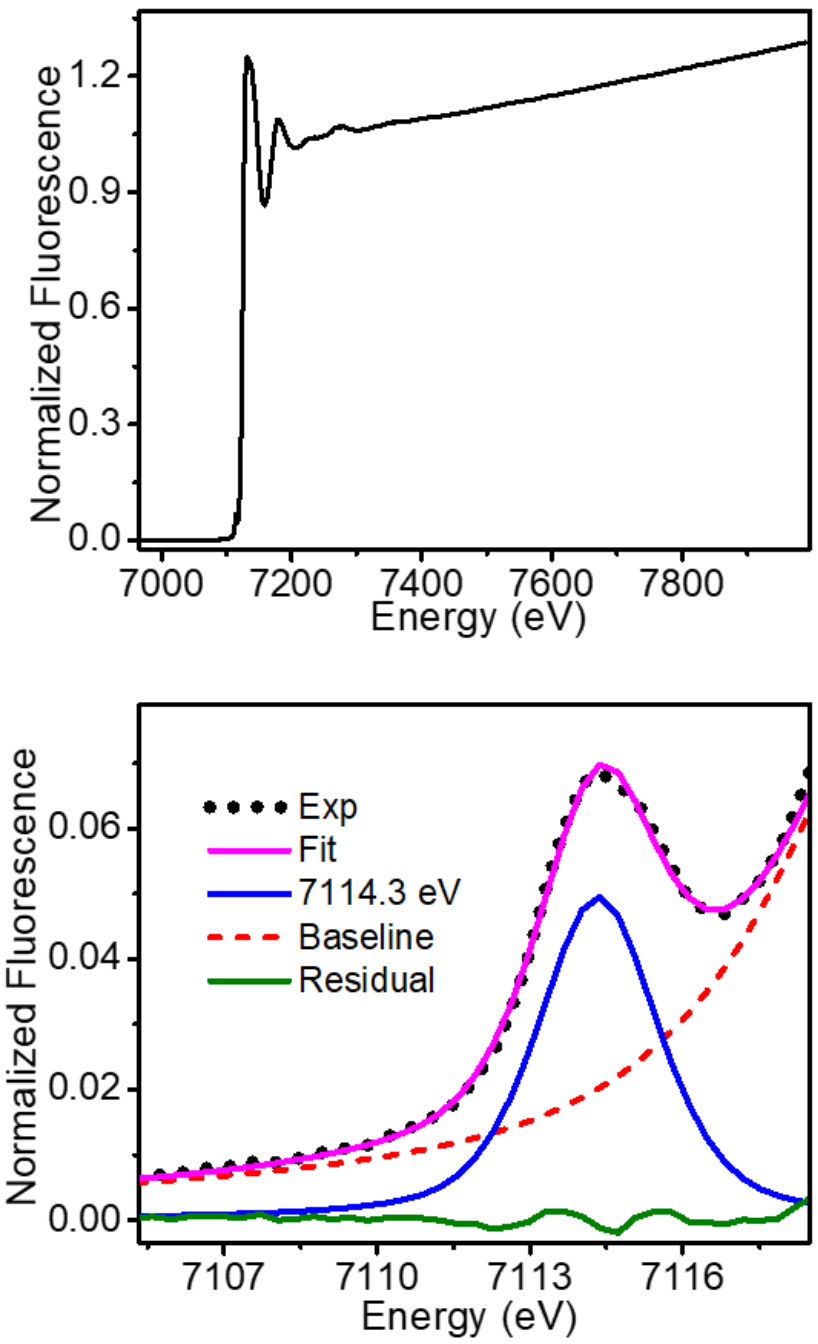

Figure S34. XAS (top) and pre-edge analysis (bottom) of decayed **2b**(CPCA) species in acetonitrile/acetone (1:3) at 10 K.

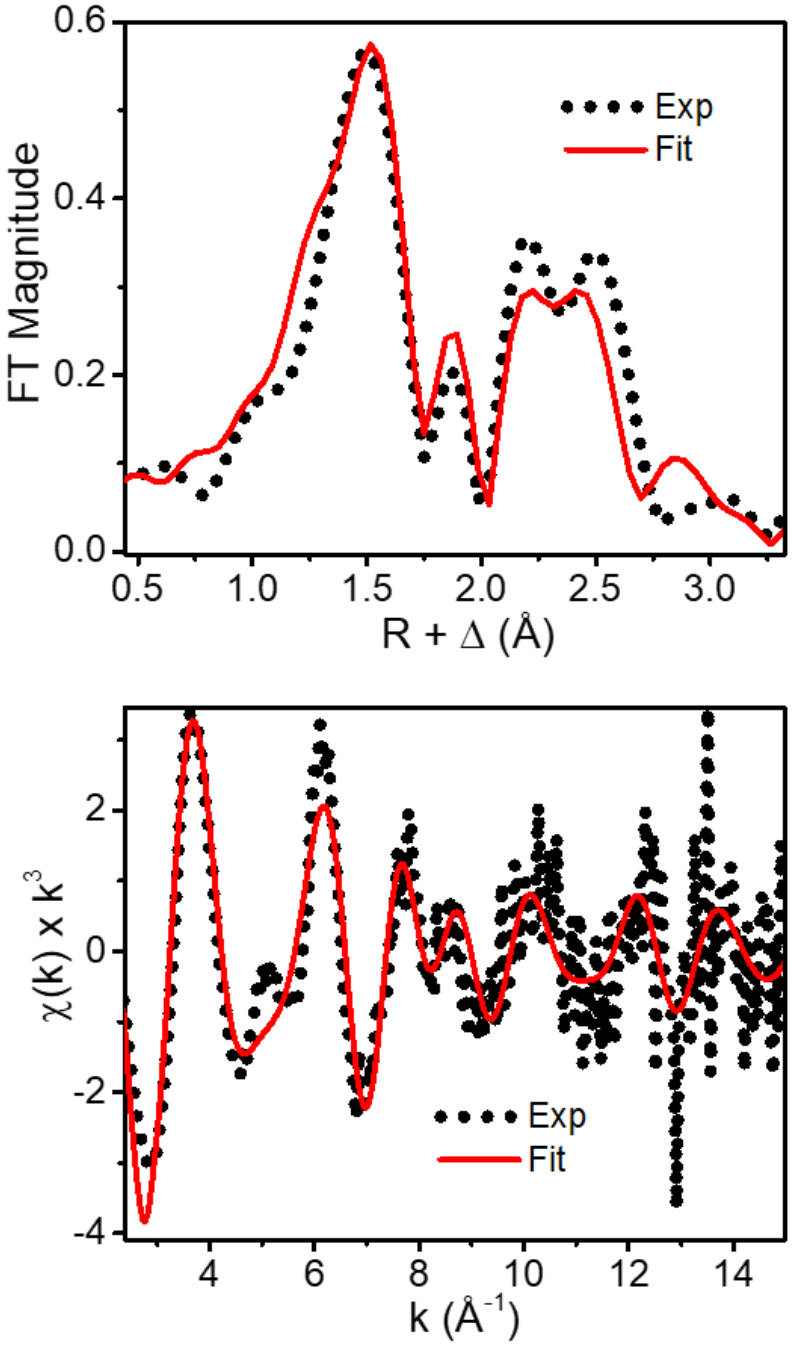

Figure S35. Unfiltered Fe K-edge EXAFS (black dotted line) and best fit (red solid line) of decayed **2b**(CPCA) species (top, Table S8, Fit 7) and corresponding unfiltered *k*-space data (black dotted line) and best fit (red solid line) (bottom).

Table S8. EXAFS fit parameters for decayed **2b**(CPCA) in acetonitrile/acetone (1:3). Fourier transformed range k = 2 - 15 Å^{-1}, resolution 0.12 Å.

	Fe–N/O			Fe–N/O			Fe···C			GOF		
Fit	N	r (Å)	σ^2 (10^{-3})	N	r (Å)	σ^2 (10^{-3})	N	r (Å)	σ^2 (10^{-3})	F	F'	E_0
1	6	2.08	17.5							233	692	-4.15
2	4	2.06	12.1							246	712	-5.2
3	3	2.05	9.3							265	739	-5.7
4	3	2.03	5.3	2	2.2	3.65				208	654	-2.45
5	3	2.01	5.4	3	2.18	6.7				204	645	-3
6	3	2.02	5.3	3	2.19	6.4	4	2.97	5.5	135	527	-1.46
7	**3**	**2.02**	**5.3**	**3**	**2.19**	**6.5**	**6**	**2.97**	**8.5**	**132**	**522**	**1.46**

Scale Factor S_0^2 = 0.9. GOF = Goodness-of-fit calculated as

$$F = \sqrt{\sum k^6 \left(\chi_{\exp} - \chi_{calc}\right)^2}$$

$$F' = \sqrt{\sum k^6 \left(\chi_{\exp} - \chi_{calc}\right)^2 / \sum k^6 \chi_{\exp}{}^2}$$

XAS analysis of 1

The Fe K-edge for **1** in acetonitrile/acetone (1:3) solution is observed at 7123.1 eV with a pre-edge feature at 7112.8 eV with a pre-edge area of 4.9 units (Figure S36). This low pre-edge area suggests that the iron center has a nearly centrosymmetric environment. The Fourier-transform-EXAFS data show two prominent features at R + Δ ~ 1.4 and 2.6 Å (Figure S37). Best fits listed in Table S9 reveal 3 N/O scatterers at 1.90 Å and 3 N/O scatterers at 2.05 Å for the first coordination sphere (Table S9). When these results are compared to those obtained from the crystal structure of **1**, with an average Fe−N_{amine} bond distance of 2.255 Å and an Fe−N_{py} distance of 2.113 Å, it is clear that the sample in frozen acetonitrile/acetone (1:3) solution at T = 10 K is not the high-spin iron(II) complex found in the crystal structure but rather its low-spin analog. This spin-state change is likely the result of the displacement of the two triflate ligands by the MeCN co-solvent in frozen solution at 10 K to give rise to the shorter Fe–N bonds typical of a low-spin iron(II) complex.

Table S9. EXAFS fit parameters for **1** in acetonitrile/acetone (1:3) solution. Fourier transformed range k = 2 - 14 $Å^{-1}$, resolution 0.13 Å.

	Fe–N/O			Fe–N/O			Fe···C			Fe···C			GOF		
Fit	N	r(Å)	σ^2 (10^{-3})	N	r(Å)	σ^2 (10^{-3})	N	r(Å)	σ^2 (10^{-3})	N	r(Å)	σ^2 (10^{-3})	F	F'	E_0
1	6	1.94	13.1										493	744	-13.2
2	4	1.94	9.4										497	757	-13.6
3	4	1.91	5.9	2	2.06	2.9							448	719	-12.6
4	4	1.92	7	2	2.08	4.4	4	2.85	0.4				204	485	-9.5
5	4	1.92	6.9	2	2.08	4.1	6	2.85	2.2				222	506	-9.5
6	4	1.92	6.7	2	209	3.7	6	2.86	2.9	4	3.14	2.9	173	447	-9.2
7	**3**	**1.90**	**4.8**	**3**	**2.05**	**5.4**	**6**	**2.85**	**2.8**	**4**	**3.14**	**2.6**	**173**	**447**	**-9.6**

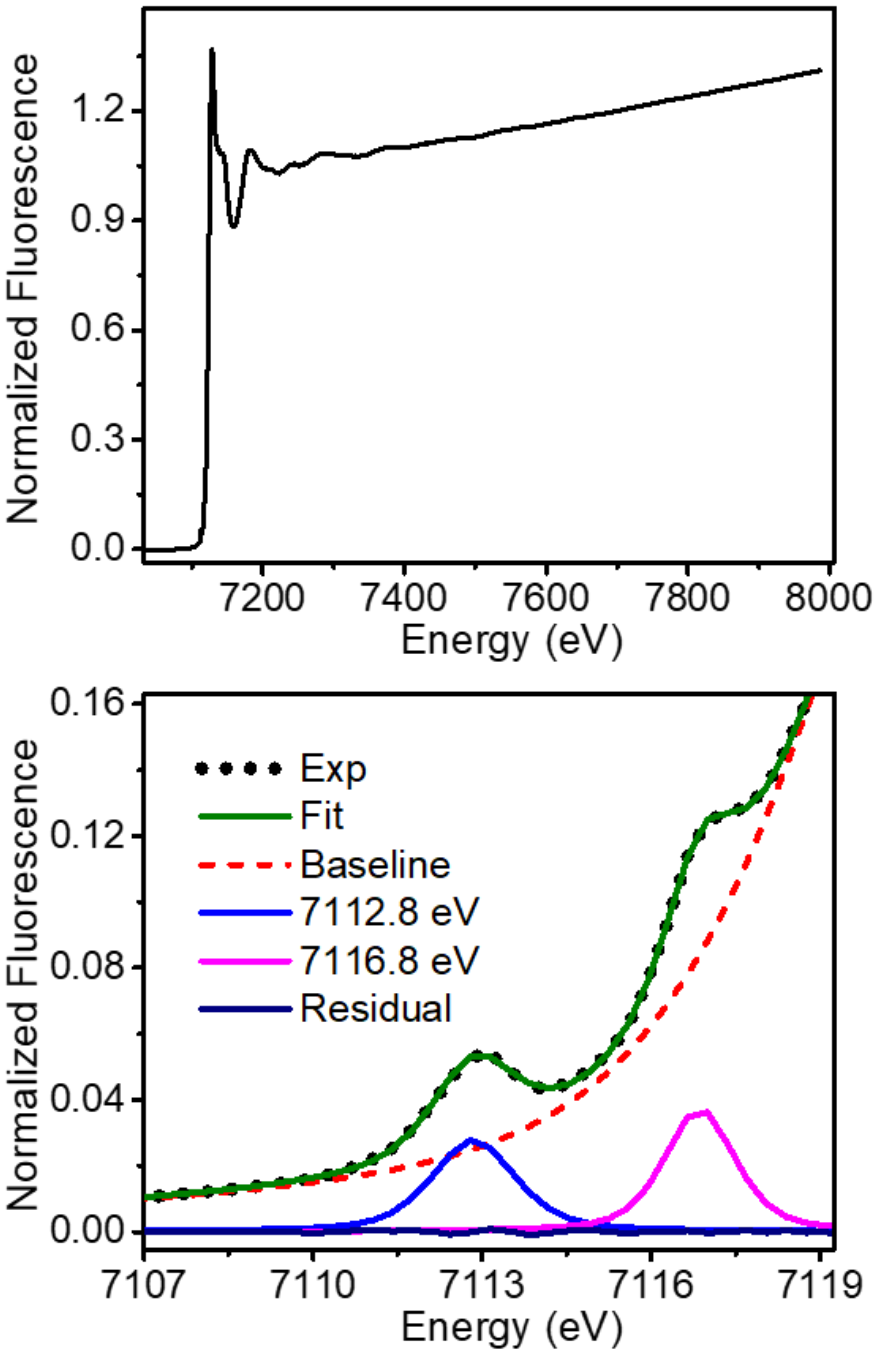

Figure S36. XAS data of **1** in acetonitrile/acetone (1:3) solution at 10 K (top) and analysis of the pre-edge region (bottom).

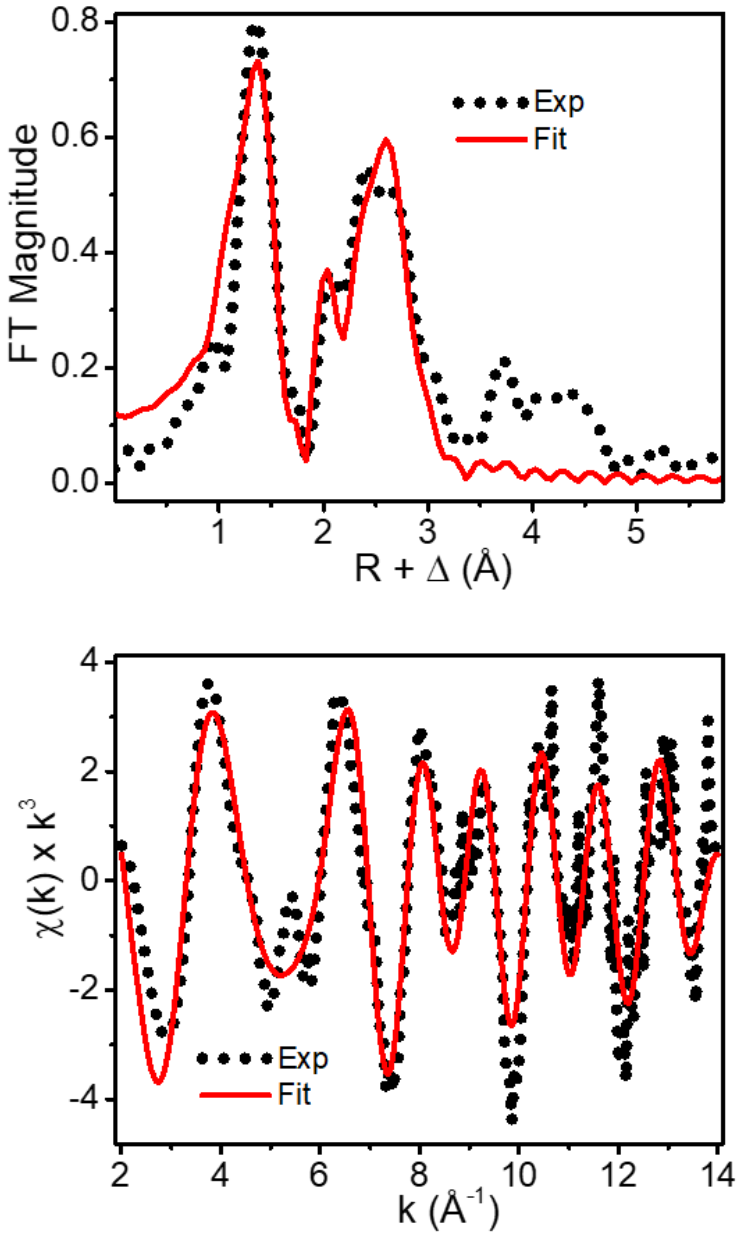

Figure S37. Unfiltered Fe K-edge EXAFS (black dotted line) and best fit (red solid line) of **1** in acetonitrile/acetone (1:3) solution at 10 K (top, Table S9, Fit 7); corresponding unfiltered k-space data (black dotted line) and best fit (red solid line) (bottom).

XII. Synthesis and characterization of species 2b(PNA) and 3b(PNA) generated with ^{18}O-labeled pernonanoic acid

Synthesis of ^{18}O-labeled nonanoic acid

^{18}O-labeled water (300 µl, 97% labeled, 16.5 mmol) was added dropwise to a stirred solution of nonanoic acid (100 mg, 0.63 mmol) in methanesulfonic acid (500 µl) at 40 ºC and was stirred for 48 h. After this time the solution was cooled with ice (approx. 1 g), followed by saturated aqueous $(NH_4)_2SO_4$ solution (1 mL). The mixture was extracted with CH_2Cl_2 (3 x 1 mL) and washed with saturated $(NH_4)_2SO_4$ solution (3 x 1 mL), dried with $MgSO_4$, filtered and concentrated by rotary evaporation. The desired product was obtained as a white oil (97 mg, 99%). ESI-MS analysis of the molecular mass peak at m/z 157 corresponding to $[C_9H_{17}O_2]^-$ revealed the following isotopic distribution: m= 0.7%, m+2= 8%, m+4= 90% (Figure S38).

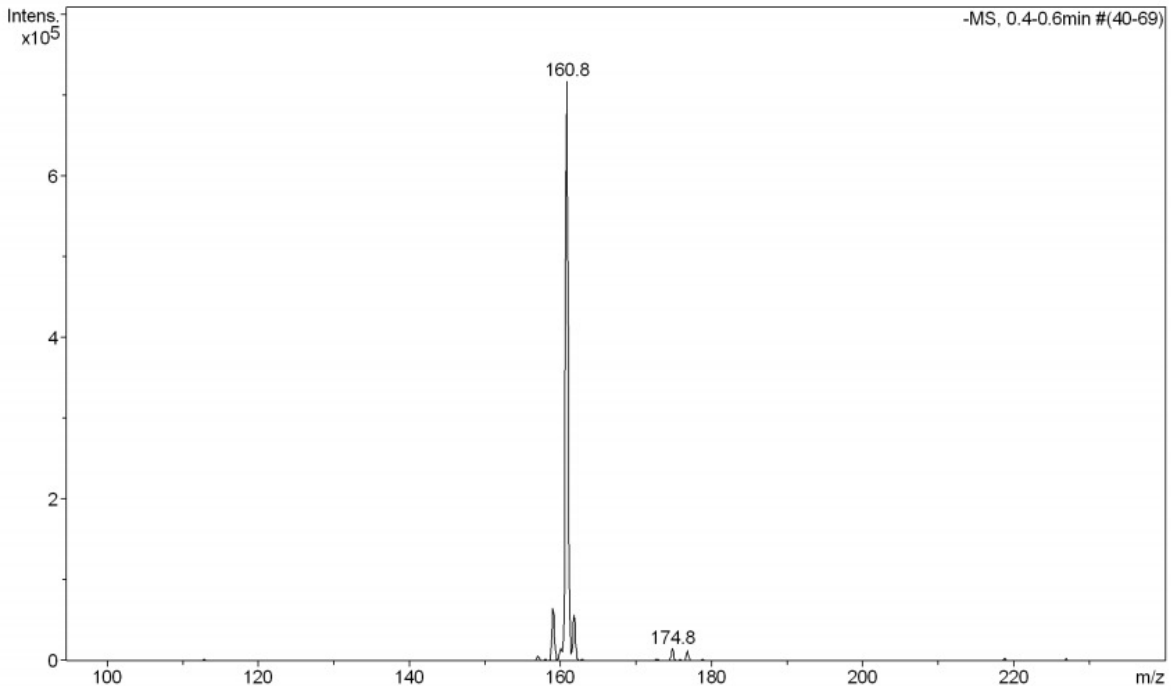

Figure S38. ESI-MS of ^{18}O-labelled nonanoic acid.

Synthesis of ^{18}O-labeled pernonanoic acid (PNA)

Synthesis method is adapted from the work of Serrano-Plana et al.[9] 95% ^{18}O-labeled hydrogen peroxide 28% w/w in water (72 µL, 0.58 mmol, obtained from Gioxcat) was added dropwise to a stirred suspension of ^{18}O-nonanoic acid (74 mg, 0.46 mmol) in methanesulfonic acid (500 µL) and ^{18}O-labeled water (92% ^{18}O content, 25 µL) at 40 ºC. The solution was stirred for 4.5 h. After this time the solution was treated with ice, followed by saturated aqueous $(NH_4)_2SO_4$ solution (1 mL). The resulting mixture was extracted with CH_2Cl_2 (3 x 1 mL), the combined extracts were washed with saturated aqueous $(NH_4)_2SO_4$ (3 x 1 mL), dried ($MgSO_4$), filtered and concentrated by rotary evaporation at room temperature (it is important not warming it up at this point). The desired product, ^{18}O-labeled pernonanoic acid (PNA), was obtained as a white crystalline solid (50 mg, 60% yield). HR-MS analysis of the molecular mass peak at m/z 173.12 corresponding to $[C_9H_{17}O_3]^-$ revealed the following isotopic distribution: m=1%, m+2 = 5%, m+4 = 19%, m+6 = 75% (Figure S39). ^{1}H-NMR ($CDCl_3$, 400 MHz, 298K) δ, ppm: 11.48 (s br, 1H, OH), 2.40 (t, J = 7.68 Hz, 2H), 1.70 (m, 2H), 1.30 (m, 10H), 0.89 (m, 3H).

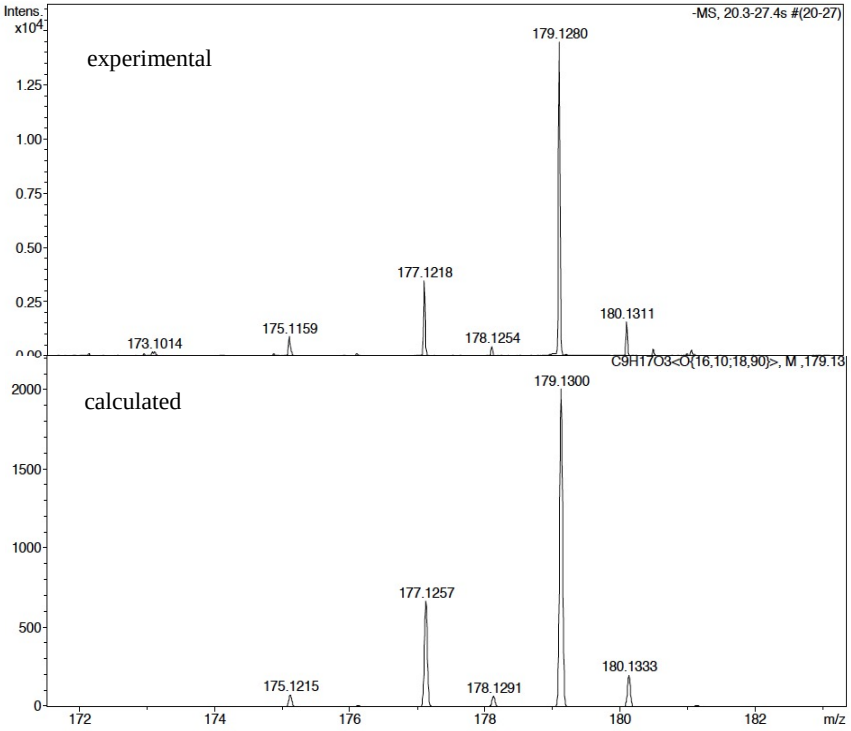

Figure S39. HR-MS of ^{18}O-labeled pernonanoic acid (PNA).

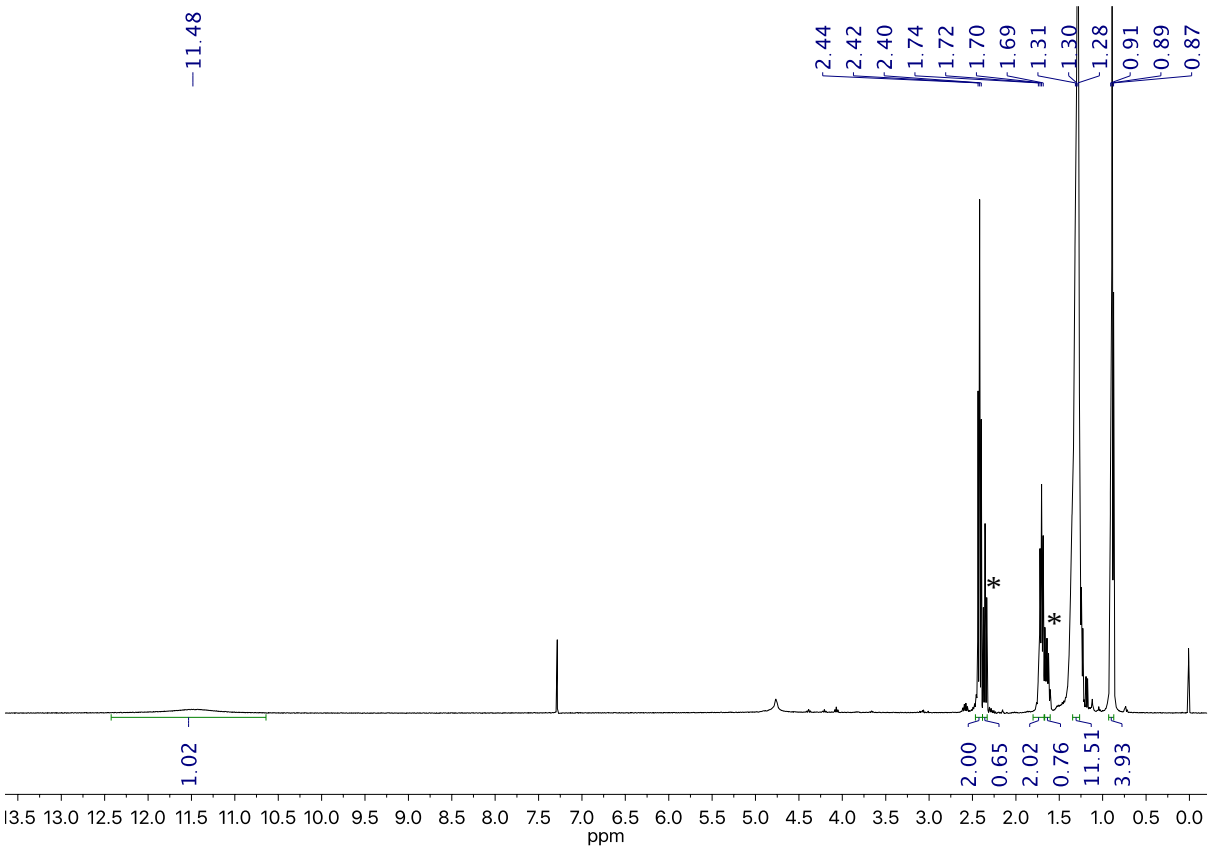

Figure S40. ^{1}H-NMR spectrum of ^{18}O-labeled pernonanoic acid in $CDCl_3$ at 298 K (*starting material).

Generation of ^{18}O-labeled 2b(PNA) and 3b(PNA) species

A 1 mM solution of **1** or [(MeO-PyNMe$_3$)Fe^{II}](CF$_3$SO$_3$)$_2$ in dry acetonitrile was prepared inside the glovebox. 2 mL of this solution were placed in a UV-Vis cuvette (2 µmols of Fe). The quartz cell was capped with a septum and taken out of the box, placed in the Unisoku cryostat of the UV-Vis spectrophotometer and cooled down to 238 K. After reaching thermal equilibrium, a UV-Vis spectrum of the starting complex was recorded. Then, 50 µL of a solution containing 5 equiv ^{18}O-labeled pernonanoic acid in dry acetonitrile were added (10 µmols). The formation of a band at λ_{max} = 496 nm for **2b**(PNA) and 512 nm for **3b**(PNA) was observed. For **2b**(PNA), cryospray ionization MS analysis (CSI-MS) at -40 ºC was carried out in order to determine the ^{18}O content of this species. The mass peak at m/z 626.20 corresponding to [Fe(PyNMe$_3$)(C$_9$H$_{17}$O$_3$)(CF$_3$SO$_3$)]$^+$ revealed the following isotopic distribution: m = 1%, m+2 = 4%, m+4 = 21%, m+6 = 73% (Figure S41).

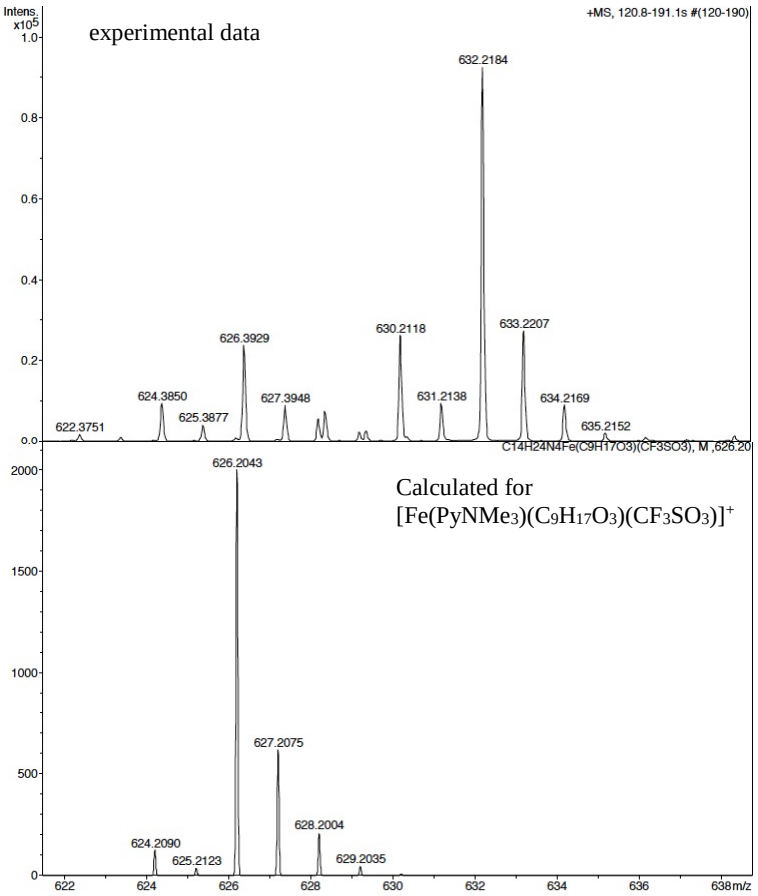

Figure S41. CSI-MS of ^{18}O-labeled **2b**(PNA) at -40 ºC showing the molecular mass peak and comparison with the calculated mass peak of the unlabeled species.

XIII. Additional information

Wiberg bond order analysis

Table S10. Wiberg bond order analysis of DFT-optimized high-valent iron-oxo/peroxo species.

Species	BO(O1-O2)	BO(Fe-O1)
3b(CPCA)	0.35	1.45
3a(CPCA)	0.84	0.84
$[(L^*)Fe^{V}(O)(NCMe)]^{3+}$	-	1.67
$[(L^*)Fe^{IV}(O)(NCMe)]^{2+}$	-	1.56
$[Fe^{V}(O)(TAML)]^{-}$	-	1.54
$[Fe^{IV}(O)(TAML)]^{2-}$	-	1.53

EPR and Mössbauer spectra of 2b(PNA)

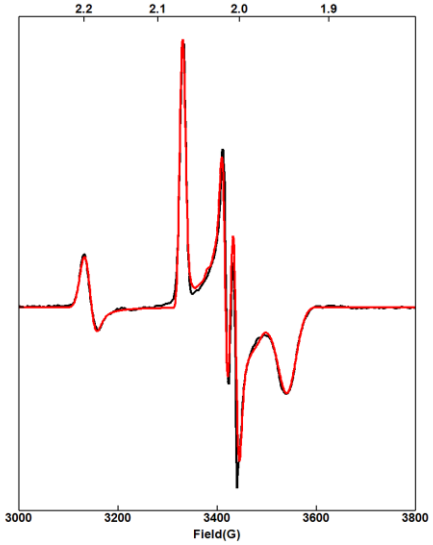

Figure S42. Wide EPR scan of the ^{57}Fe sample of **2**(PNA) (^{57}Fe concentration 2 mM) at T = 15 K. The black curve indicates the experimental data and the red curve indicates the simulation result by the following two sets of parameters: species **2b**(PNA): $g_{x,y,z}$ = [2.01, 2.07, 1.94], $\sigma(g_z)$ = 0.009, $A_{x,y,z}$ = [62(2), 6(4), 11(4)] MHz, spin concentration = 1.02 mM; species **2a**(PNA): $g_{x,y,z}$ = [2.20, 2.19, 1.98], spin concentration = 0.11 mM.

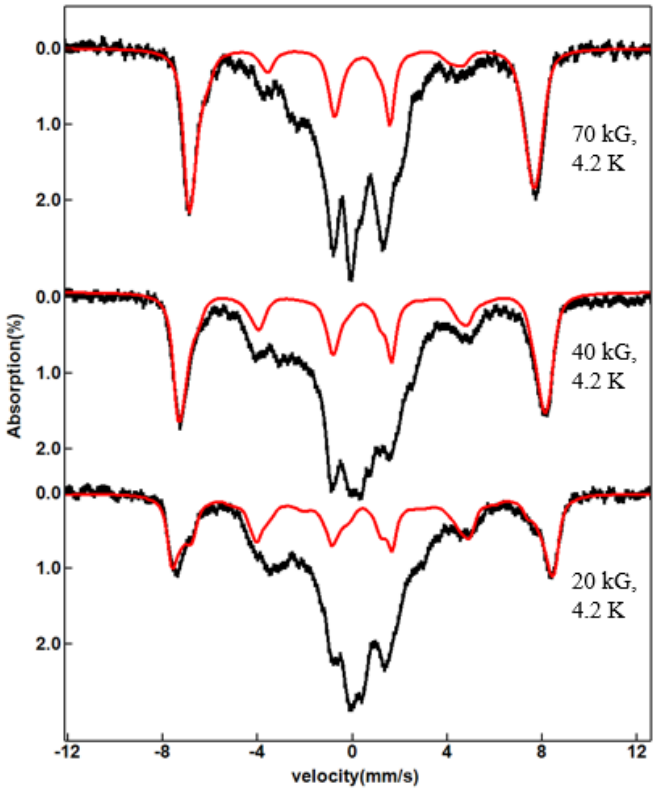

Figure S43. 7.0/4.0/2.0 T spectra of **2b**(PNA) at 4.2 K. The experimental spectra are indicated by black color and the simulated spectra are indicated by red. Two sites are used to simulate these spectra: HS-ferric species #1: D = 0.7 cm^{-1}, E/D=0.16, ΔE_Q = -1.0 mm/s, η = 2.0, $A_x/g_n\beta_n$ = -21.0 T, $A_y/g_n\beta_n$ = -19.8 T, $A_z/g_n\beta_n$ = -19.0 T, δ = 0.41 mm/s, percentage = 12%; HS-ferric species #2: D = 0.7 cm^{-1}, E/D=0.23, ΔE_Q = 0.36 mm/s, η = -1.7, $A_x/g_n\beta_n$ = -20.0 T, $A_y/g_n\beta_n$ = -21.2 T, $A_z/g_n\beta_n$ = -22.0 T, δ = 0.41 mm/s, percentage = 28%.

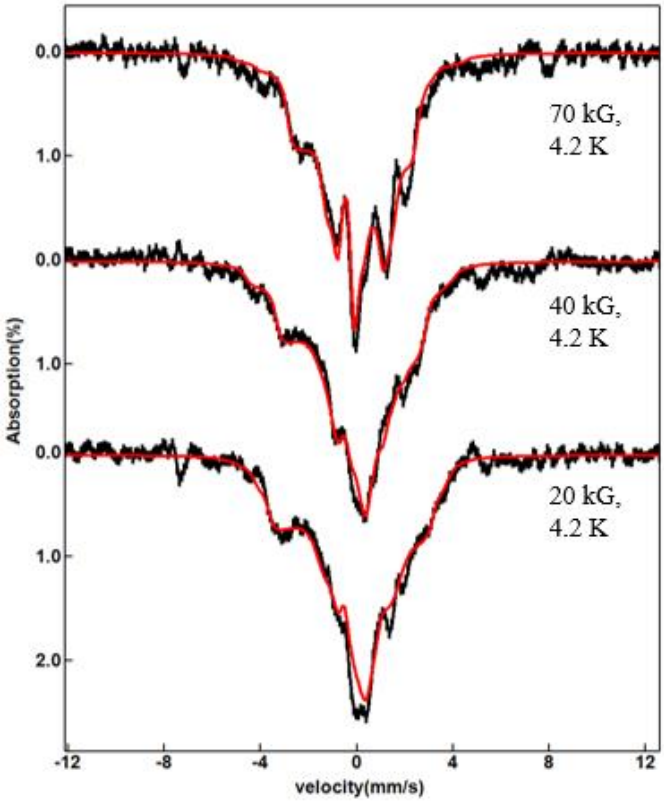

Figure S44. 7.0/4.0/2.0 T spectra of **2b**(PNA) at 4.2 K with HS-ferric removed. The simulation results are indicated by red. Three species are applied to simulate the spectra: **2b**(PNA)(S=1/2): ΔE_Q = -1.11 mm/s, η = 0.3, $A_x/g_n\beta_n$ = -62.0 MHz, $A_y/g_n\beta_n$ = -7.5 MHz, $A_z/g_n\beta_n$ = -8.9 MHz, δ = -0.08 mm/s, percent = 49%; **2a**(PNA)(S=1/2): ΔE_Q = -1.40 mm/s, η = 0.0, $A_x/g_n\beta_n$ = +8.0 MHz, $A_y/g_n\beta_n$ = +9.7 MHz, $A_z/g_n\beta_n$ = -82.3 MHz, δ = 0.17 mm/s, percent = 5%; di-ferric(S=0): ΔE_Q = 0.28 mm/s, η = 0.2, δ = 0.40 mm/s, percent = 3%.

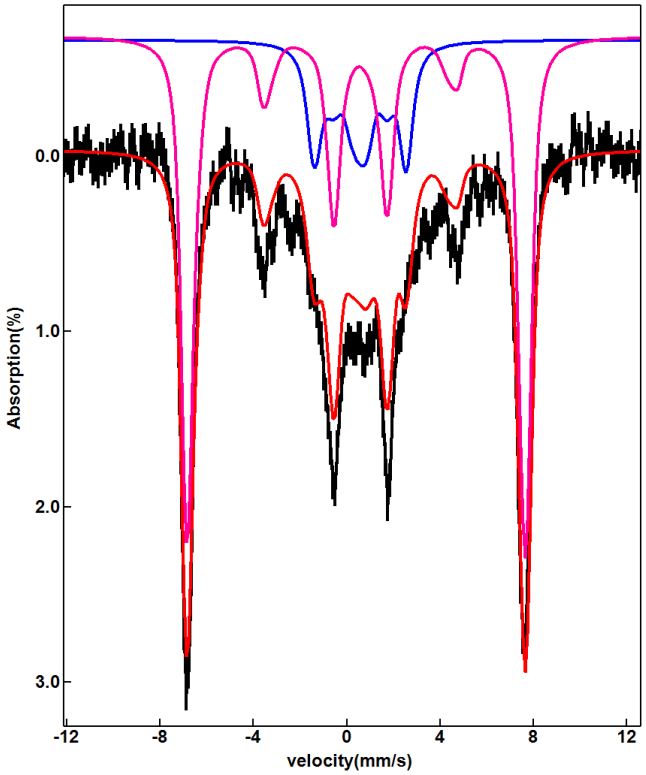

Figure S45. 7.0 T spectra of decayed sample of **2**(PNA) at 4.2 K. The experimental spectra are indicated by black color and the simulated spectra are indicated by red. Two sites are used to simulate these spectra: HS-ferric species (purple): D = 0.7 cm^{-1}, E/D=0.23, ΔE_Q = 0.94 mm/s, η = -0.8, $A_x/g_n\beta_n$ = -20.8 T, $A_y/g_n\beta_n$ = -20.8 T, $A_z/g_n\beta_n$ = -20.4 T, δ = 0.49 mm/s, percentage = 66%; di-ferric species (blue): ΔE_Q = -2.13 mm/s, η = 0.8, δ = 0.55 mm/s, percentage = 25%.

Additional DFT Results

Table S11. DFT energies[a] of Fe^{IV} and Fe^{V} states of [Fe(O)TAML] and [Fe(O)(MeO-PyNMe$_3$)(MeCN)] complexes

Species, Spin	PCM model[b]	Electronic energy (Hartree)	Relative energy (kcal/mol)
$[Fe^{IV}(O)TAML]^{2-}$, $S = 1$	No	-2596.5190	0
$[Fe^{V}(O)TAML]^{-}$, $S = 1/2$	No	-2596.5323	–8.3[b,c]
$[Fe^{IV}(O)(MeO\text{-}PyNMe_3)(MeCN)]^{2+}$, $S = 1$	No	-2352.8895	0
$[Fe^{V}(O)(MeO\text{-}PyNMe_3)(MeCN)]^{3+}$, $S = 1/2$	No	-2352.3890	+313.8[c]
$[Fe^{IV}(O)TAML]^{2-}$, $S = 1$	MeCN	-2596.7438	0
$[Fe^{V}(O)TAML]^{-}$–, $S = 1/2$	MeCN	-2596.5977	**+91.6**[d]
$[Fe^{IV}(O)(MeO\text{-}PyNMe_3)(MeCN)]^{2+}$, $S = 1$	MeCN	-2353.1031	0
$[Fe^{V}(O)(MeO\text{-}PyNMe_3)(MeCN)]^{3+}$, $S = 1/2$	MeCN	-2352.8543	**+156.0**[d]

[a] BP86/6-311G electronic energies for optimized geometries.

[b] The negative sign implies that the Fe^{IV}TAML complex is predicted to spontaneously lose an electron in gas phase. The Fe^{IV} state is stable when the TAML complex is immersed in acetonitrile (see bottom halve of table).

[c] The relative energy for the MeO-PyNMe$_3$$Fe^{IV}$ complex (last column) is much higher than for the TAMLFe^{IV} complex, which implies that former species is predicted to be more electrophilic than the latter.

[d] Upon reduction of the Fe^{V} species the molecular charge changes from –1 to –2 in the case of TAML complex and from 3+ to 2+ in the case of the MeO-PyNMe3 complex; hence, the 1e$^-$ reduction of the two species, respectively, increases and decreases the magnitude of the molecular charge (z). Since according to Born's expression for the solvation energy,

$\Delta G = -\frac{N_A z^2 e^2}{8\pi\varepsilon_0 r_0}(1-\frac{1}{\epsilon_r})$, the solvation energy depends on z^2, the solvation energy increases in the 1e$^-$ reduction of the TAML species but decreases in the reduction of the MeO-PyNMe$_3$ complex. These changes result in a smaller difference between the relative energies for the two species. The polarizable continuum model (PCM) for calculating the solvation energy predicts that this difference is reduced from 332.1 kcal/mol (in gas phase)

to 64.4 kcal/mol (in MeCN). Thus, both in the absence and presence of the MeCN solvent the $[Fe^{V}(O)(MeO\text{-}PyNMe_3)(MeCN)]^{3+}$ complex is predicted to be more electrophilic than the $[Fe^{V}(O)TAML]^{-}$ complex, which may be one of the reasons for the greater reactivity of the former species (see main text).

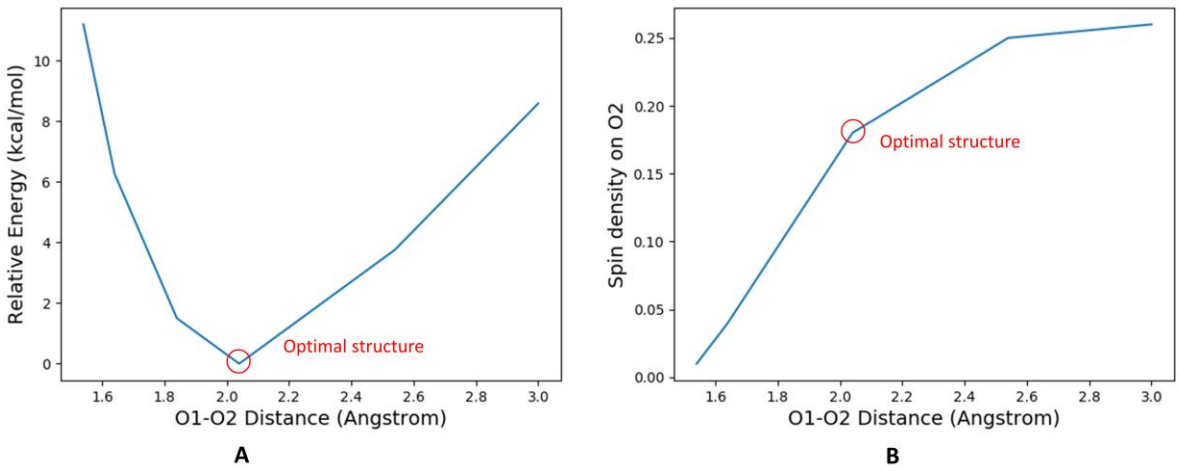

Figure S46. (A) Relative energy (to the optimal structure with r(O1–O2)=2.04 Å) and (B) spin density on O2 versus the O1–O2 distance. (This Figure has been added in the SI as Figure S46)

Table S12. DFT-derived xyz coordinates

3a(CPCA) cis isomer

Fe	-0.82817700	-0.01593900	-0.05241400
O	-0.89882900	-0.11703200	-1.87600400
N	1.07754700	0.10084500	-0.23995100
C	1.81688600	-1.03289100	-0.28028100
O	-2.80629000	-0.15575900	-0.17490000
N	-0.69261000	2.06450500	0.02024200
N	-0.81388700	0.08708000	2.00999800
N	-0.41350000	-2.04336300	0.22488500
C	3.02382000	1.44777700	-0.50219900
H	3.50901100	2.40363200	-0.62748600
C	1.65562700	1.32451700	-0.40102900
C	0.65361400	2.42662600	-0.59405100
H	0.49168300	2.54594300	-1.66587800
H	0.99650800	3.38480200	-0.20239500
C	-1.77477400	2.78048000	-0.75117300
H	-1.61624500	3.85911300	-0.70851600
H	-2.74047300	2.54828900	-0.31313600
H	-1.74976400	2.45581400	-1.78679200
C	-0.75537400	2.48343600	1.48177300
H	-1.80120700	2.64945600	1.72674600
H	-0.23819900	3.43457900	1.61703300
C	-0.15750700	1.40145300	2.36377300
H	0.91285700	1.30255600	2.20011100
H	-0.31446900	1.63192500	3.41963600
C	-2.19670800	0.03417600	2.61758800
H	-2.11622500	0.09877600	3.70348600
H	-2.69685200	-0.88631900	2.34291200
H	-2.80468700	0.85022100	2.24739300
C	-0.00590300	-1.09478000	2.49301300
H	-0.14966300	-1.23901000	3.56588900
H	1.04674900	-0.88036800	2.32466500
C	-0.45306800	-2.32261600	1.71963000
H	0.17129700	-3.18674700	1.95225800
H	-1.47586000	-2.58859800	1.97323800
C	-1.37645800	-2.96689900	-0.48170900
H	-1.37662600	-2.73768500	-1.54283300
H	-2.37207700	-2.82608900	-0.07270900
H	-1.07730500	-4.00607600	-0.33645100
C	-3.22830800	-0.24289000	-1.37677700
C	3.82142600	0.27997200	-0.47282900
C	3.19940100	-0.98366100	-0.38243100
H	3.77434100	-1.89565800	-0.41295300

C	0.98206400	-2.28194300	-0.33722900
H	1.44778300	-3.12670100	0.17179300
H	0.86131900	-2.55505600	-1.38612600
O	-2.35109000	-0.23602400	-2.38423800
O	5.14942000	0.48440600	-0.56064100
C	6.11592900	-0.63229900	-0.59467200
H	7.08023900	-0.14728300	-0.67110500
H	5.93721800	-1.25506600	-1.46968500
H	6.05596400	-1.20880600	0.32716600
C	-4.65474100	-0.34884000	-1.76816100
H	-4.76014400	-0.51514200	-2.83588300
H	-5.12744500	-1.16398000	-1.21952400
H	-5.17922700	0.56998500	-1.49747500

3b(CPCA) trans isomer

Fe	-0.00726100	-0.00633300	0.00774500
N	0.08435201	0.00567300	-1.97574415
C	0.18745301	1.20096209	-2.62659720
O	-0.00516400	-0.01675900	1.66021913
N	-0.14683701	-2.05808916	-0.31766402
N	-2.07586916	-0.00267700	-0.01947500
N	-0.14034901	2.04986016	-0.29272902
C	0.25057202	-1.20235709	-4.04047731
H	0.31583402	-2.14706116	-4.57913135
C	0.18200101	-1.18180409	-2.64153620
C	0.36899603	-2.36128518	-1.72356113
H	1.45065811	-2.54674919	-1.63462612
H	-0.09587701	-3.28463725	-2.10224816
C	0.63364905	-2.88080222	0.68755205
H	0.46303204	-3.95365630	0.50961104
H	0.31302302	-2.61028920	1.69810913
H	1.69991113	-2.66025620	0.57767604
C	-1.63255213	-2.40891619	-0.20967802
H	-1.84214814	-2.59024820	0.85162407
H	-1.83115014	-3.34857725	-0.74822706
C	-2.48561619	-1.26746710	-0.74952706
H	-2.32990318	-1.11491808	-1.82509414
H	-3.55628027	-1.47046511	-0.58663004
C	-2.69965820	-0.00870400	1.36866311
H	-3.79532729	-0.00631800	1.26949010
H	-2.37552418	0.86787507	1.93456215
H	-2.37848218	-0.89220707	1.92542215
C	-2.48116119	1.27079510	-0.73664606
H	-3.55137127	1.47533011	-0.57265104
H	-2.32483918	1.12882208	-1.81353814
C	-1.62528613	2.40418818	-0.18431601
H	-1.81987414	3.34957325	-0.71424305
H	-1.83642814	2.57628120	0.87823307
C	0.64020505	2.85771322	0.72436105
H	1.70611713	2.63595620	0.61376105
H	0.31703402	2.57486420	1.73076613
H	0.47260304	3.93318630	0.55989504
C	0.25617902	1.23870409	-4.02511731
H	0.32589202	2.18973417	-4.55195935
C	0.38007703	2.36770518	-1.69365013
H	-0.07827101	3.29863725	-2.06156416
H	1.46276411	2.54495419	-1.60018112
O	1.91633915	-0.00882500	-0.06055100
O	1.94889115	-0.02155300	2.23285317

C	2.57070920	-0.01658500	1.10929108
C	4.66357836	-1.30603810	1.73352413
H	4.33354733	-1.33755010	2.78512521
H	4.26684533	-2.20630917	1.23406609
C	4.09186031	-0.01956300	1.06381008
H	4.35669633	-0.01662000	-0.00727600
C	6.20944548	-1.30054910	1.65965612
H	6.53092452	-1.36946210	0.60466304
H	6.59026752	-2.20352817	2.16235916
C	6.80206351	-0.02907800	2.30308117
H	7.89763558	-0.03106300	2.19583517
H	6.59044850	-0.03203800	3.38696926
C	6.21483245	1.24885310	1.66764913
H	6.53656148	1.32304810	0.61309504
H	6.59940048	2.14707117	2.17600516
C	4.66895136	1.26036510	1.74162914
H	4.27599533	2.16538516	1.24779610
H	4.33919533	1.28656510	2.79347421
C	0.25719202	0.02255900	-4.73426736
H	0.29624002	0.02932600	-5.82326944

3b(CPCA) cis isomer

Fe	0.20214902	0.06044600	0.02736500
O	-0.14275101	-0.04902100	-1.58642112
N	2.09469316	0.06973801	-0.32380502
C	2.76024121	-1.11779708	-0.43854803
O	-1.66842613	0.05886800	0.47451304
N	0.46271004	2.12554516	0.05400600
N	0.57510004	0.20010402	2.14094916
N	0.53409804	-1.97395915	0.31139002
C	4.08299631	1.30485910	-0.83630706
H	4.60693935	2.23615217	-1.04493508
C	2.72014421	1.26467910	-0.58574704
C	1.74675313	2.40399918	-0.72983806
H	1.46108611	2.47426319	-1.79107714
H	2.16543517	3.37602726	-0.42863003
C	-0.67657505	2.88589522	-0.58922104
H	-0.45687304	3.96466930	-0.59431705
H	-1.59049012	2.70447620	-0.01506000
H	-0.81175206	2.52613819	-1.61433913
C	0.62307205	2.56865520	1.50866012
H	-0.38518003	2.74836821	1.90044414
H	1.16429909	3.52743127	1.54179812
C	1.33928510	1.49486911	2.32128218
H	2.37070918	1.34672110	1.97779215
H	1.37654811	1.77873713	3.38591926
C	-0.66355505	0.23638702	3.01511023
H	-0.35522903	0.31563402	4.06941831
H	-1.26154110	-0.66493605	2.86794122
H	-1.29684610	1.08384508	2.74681521
C	1.37865510	-1.03520508	2.48362819
H	1.41698511	-1.18241409	3.57553027
H	2.40724918	-0.89530207	2.12831116
C	0.70375705	-2.22646317	1.81014314
H	1.27759810	-3.15423724	1.96342015
H	-0.29960202	-2.39043418	2.22122217
C	-0.57493904	-2.84673522	-0.23463602
H	-0.71904706	-2.61647120	-1.29528110
H	-1.49714311	-2.62975920	0.31303402
H	-0.31805402	-3.91001530	-0.11024201
C	-2.54935020	-0.01849800	-0.53071204
C	4.81586437	0.08489101	-0.86094806
C	4.13192932	-1.14890809	-0.68963005
H	4.64951836	-2.10177216	-0.78027406
C	1.83003514	-2.30280418	-0.43146603
H	2.28322317	-3.21193925	-0.00774900

H	1.55144912	-2.52025019	-1.47469411
O	-2.17462717	-0.08604601	-1.75647013
O	6.14679349	0.21664802	-1.09037908
C	7.02970652	-0.97911207	-1.19784109
H	8.02145459	-0.55818704	-1.37229710
H	6.72257749	-1.59735012	-2.05181915
H	7.01530454	-1.54540912	-0.25696202
C	-4.03063031	-0.03679000	-0.17624401
H	-4.07974831	0.11579101	0.91525607
C	-4.79755137	1.11045608	-0.89746207
H	-4.67967636	0.98729507	-1.98690115
H	-4.36408833	2.08831516	-0.62859805
C	-4.65293435	-1.42443011	-0.52611804
H	-4.11848731	-2.22906417	0.00701500
H	-4.53411135	-1.60502212	-1.60748412
C	-6.29619345	1.07300608	-0.51536904
H	-6.82037755	1.87516714	-1.05823208
H	-6.41151150	1.29617610	0.56083104
C	-6.15309747	-1.44469911	-0.14529101
H	-6.57480850	-2.42250019	-0.42716203
H	-6.25820350	-1.36138010	0.95150807
C	-6.92718552	-0.29974902	-0.83143506
H	-6.93103253	-0.46073904	-1.92406115
H	-7.97916459	-0.31223702	-0.50740304

3b(PAA) trans isomer

Fe	0.00938700	-0.00568800	-0.00923900
N	0.08221300	0.01272400	-1.97882900
C	0.16882100	1.20329700	-2.64358900
O	-0.00375100	-0.01492300	1.64436000
N	-0.12497000	-2.05560200	-0.33746500
N	-2.06011000	-0.00679100	-0.02855400
N	-0.12537300	2.05196500	-0.30719000
C	0.21118400	-1.20423700	-4.04476500
H	0.27934100	-2.13353900	-4.60809500
C	0.17631500	-1.17746700	-2.65957100
C	0.40202800	-2.35042700	-1.74151900
H	1.48841900	-2.50003600	-1.64817300
H	-0.03497500	-3.28864700	-2.11602400
C	0.65275900	-2.88003100	0.66863000
H	0.47655800	-3.95216400	0.49214200
H	0.33456400	-2.60743700	1.67945100
H	1.72017200	-2.66758500	0.55489400
C	-1.61046000	-2.41111800	-0.23893200
H	-1.82377900	-2.60566600	0.81934600
H	-1.80338000	-3.34485700	-0.78956100
C	-2.46567400	-1.26675600	-0.76974100
H	-2.30815200	-1.10504900	-1.84334900
H	-3.53585500	-1.47376000	-0.60872800
C	-2.68008700	-0.02704400	1.36042300
H	-3.77599500	-0.02809200	1.26393700
H	-2.35843700	0.84595800	1.93347300
H	-2.35495700	-0.91425800	1.90901200
C	-2.46874500	1.27223400	-0.73369000
H	-3.53782500	1.47567600	-0.56146900
H	-2.31783900	1.13778500	-1.81212500
C	-1.60926800	2.40161900	-0.17834100
H	-1.81156500	3.35241800	-0.69570200
H	-1.80861300	2.56181600	0.88836000
C	0.66730400	2.85863000	0.70151800
H	1.73249600	2.64478800	0.57070300
H	0.36137200	2.56973700	1.71168200
H	0.49144000	3.93405500	0.54560900
C	0.19025600	0.02866700	-4.75622400
C	0.20672300	1.25409500	-4.03677400
H	0.27456500	2.21094500	-4.55076400
C	0.37727600	2.37222900	-1.71444400
H	-0.08661600	3.30401600	-2.07302900
H	1.46092900	2.54802200	-1.63417100
O	0.19343200	-0.08493900	-6.10785300

C	0.21051700	1.12309700	-6.98184700
H	0.19168600	0.71491800	-7.99383800
H	1.13487900	1.69233400	-6.81700300
H	-0.68391600	1.73322200	-6.79861000
O	1.93408700	-0.00783700	-0.04366300
O	1.92818600	-0.02401700	2.24965700
C	2.56905700	-0.01838900	1.13098000
C	4.07072000	-0.02570500	1.12740100
H	4.44401600	-0.92671300	1.63613200
H	4.44480300	0.00164800	0.09872100
H	4.45424400	0.83817100	1.68940200

2b(CPCA) trans isomer

Fe	-0.00726100	-0.00633300	0.00774500
N	0.08435201	0.00567300	-1.97574415
C	0.18745301	1.20096209	-2.62659720
O	-0.00516400	-0.01675900	1.66021913
N	-0.14683701	-2.05808916	-0.31766402
N	-2.07586916	-0.00267700	-0.01947500
N	-0.14034901	2.04986016	-0.29272902
C	0.25057202	-1.20235709	-4.04047731
H	0.31583402	-2.14706116	-4.57913135
C	0.18200101	-1.18180409	-2.64153620
C	0.36899603	-2.36128518	-1.72356113
H	1.45065811	-2.54674919	-1.63462612
H	-0.09587701	-3.28463725	-2.10224816
C	0.63364905	-2.88080222	0.68755205
H	0.46303204	-3.95365630	0.50961104
H	0.31302302	-2.61028920	1.69810913
H	1.69991113	-2.66025620	0.57767604
C	-1.63255213	-2.40891619	-0.20967802
H	-1.84214814	-2.59024820	0.85162407
H	-1.83115014	-3.34857725	-0.74822706
C	-2.48561619	-1.26746710	-0.74952706
H	-2.32990318	-1.11491808	-1.82509414
H	-3.55628027	-1.47046511	-0.58663004
C	-2.69965820	-0.00870400	1.36866311
H	-3.79532729	-0.00631800	1.26949010
H	-2.37552418	0.86787507	1.93456215
H	-2.37848218	-0.89220707	1.92542215
C	-2.48116119	1.27079510	-0.73664606
H	-3.55137127	1.47533011	-0.57265104
H	-2.32483918	1.12882208	-1.81353814
C	-1.62528613	2.40418818	-0.18431601
H	-1.81987414	3.34957325	-0.71424305
H	-1.83642814	2.57628120	0.87823307
C	0.64020505	2.85771322	0.72436105
H	1.70611713	2.63595620	0.61376105
H	0.31703402	2.57486420	1.73076613
H	0.47260304	3.93318630	0.55989504
C	0.25617902	1.23870409	-4.02511731
H	0.32589202	2.18973417	-4.55195935
C	0.38007703	2.36770518	-1.69365013
H	-0.07827101	3.29863725	-2.06156416
H	1.46276411	2.54495419	-1.60018112
O	1.91633915	-0.00882500	-0.06055100
O	1.94889115	-0.02155300	2.23285317

C	2.57070920	-0.01658500	1.10929108
C	4.66357836	-1.30603810	1.73352413
H	4.33354733	-1.33755010	2.78512521
H	4.26684533	-2.20630917	1.23406609
C	4.09186031	-0.01956300	1.06381008
H	4.35669633	-0.01662000	-0.00727600
C	6.20944548	-1.30054910	1.65965612
H	6.53092452	-1.36946210	0.60466304
H	6.59026752	-2.20352817	2.16235916
C	6.80206351	-0.02907800	2.30308117
H	7.89763558	-0.03106300	2.19583517
H	6.59044850	-0.03203800	3.38696926
C	6.21483245	1.24885310	1.66764913
H	6.53656148	1.32304810	0.61309504
H	6.59940048	2.14707117	2.17600516
C	4.66895136	1.26036510	1.74162914
H	4.27599533	2.16538516	1.24779610
H	4.33919533	1.28656510	2.79347421
C	0.25719202	0.02255900	-4.73426736
H	0.29624002	0.02932600	-5.82326944

2b(CPCA) cis isomer

Fe	0.64283400	0.02491100	-0.07111100
O	0.17196200	0.07761700	-1.65963900
N	2.49929200	-0.02118900	-0.60496600
C	3.07835500	-1.22851000	-0.87582800
O	-1.18795300	0.07272100	0.51636400
N	1.01498800	2.06663300	0.10962700
N	1.20026900	-0.04345100	1.99647700
N	0.88437400	-2.04343700	0.00734700
C	4.49402000	1.15382600	-1.21781200
H	5.02325300	2.09057200	-1.38844300
C	3.15016300	1.16006400	-0.82376900
C	2.23740600	2.35488400	-0.76158700
H	1.86536100	2.54824100	-1.78059400
H	2.74124200	3.26853000	-0.41143400
C	-0.13441300	2.93298100	-0.35937700
H	0.14272200	3.99670900	-0.29917600
H	-1.00133300	2.74753800	0.28224800
H	-0.38135500	2.66777900	-1.39250500
C	1.32776400	2.36861400	1.57666100
H	0.37026700	2.56535500	2.07369100
H	1.92546400	3.29143700	1.64218800
C	2.04752100	1.19044900	2.22472800
H	3.03805200	1.02412400	1.78229100
H	2.18818800	1.37116500	3.30308700
C	0.03604400	-0.02558400	2.96881100
H	0.42790800	-0.06459500	3.99699900
H	-0.62621300	-0.87401600	2.78757600
H	-0.56209200	0.87680800	2.83058400
C	1.95951500	-1.34278500	2.16435600
H	2.08501300	-1.58428900	3.23261800
H	2.96040100	-1.22479600	1.72918400
C	1.16102300	-2.43460600	1.46016900
H	1.68859000	-3.40111600	1.48635400
H	0.18713400	-2.58090800	1.94217500
C	-0.31057000	-2.81373500	-0.51157000
H	-0.52657000	-2.49017300	-1.53488600
H	-1.17310200	-2.60144600	0.12760600
H	-0.10156500	-3.89449500	-0.49433700
C	-2.13370500	0.11296900	-0.42898500
C	4.42112200	-1.28590800	-1.27012700
H	4.89368500	-2.24447800	-1.48116900
C	2.09602000	-2.36843000	-0.86636400
H	2.54200900	-3.32327300	-0.54913500
H	1.72299500	-2.49996900	-1.89477500

O	-1.83808900	0.13540900	-1.68022900
C	-3.59085100	0.10986900	0.01297400
H	-3.57136400	0.23172700	1.10933800
C	-4.38671400	1.28107300	-0.63255600
H	-4.32858000	1.18881400	-1.73002500
H	-3.93065200	2.24764600	-0.36104800
C	-4.24503400	-1.26552700	-0.33475100
H	-3.69132200	-2.08666600	0.15128000
H	-4.18741800	-1.42084000	-1.42506500
C	-5.86295100	1.24439500	-0.17223900
H	-6.40776100	2.06451100	-0.66547600
H	-5.92034600	1.44001600	0.91397200
C	-5.72299800	-1.28214700	0.12586800
H	-6.16688400	-2.24982700	-0.15732100
H	-5.76866400	-1.22584000	1.22839500
C	-6.52158000	-0.11493300	-0.48994400
H	-6.58413300	-0.24774900	-1.58454900
H	-7.55505900	-0.12811400	-0.11119700
C	5.13722600	-0.08269100	-1.41609900
H	6.18444600	-0.10752600	-1.71628300

Complex 4

Fe	0.86675300	-0.01364600	-0.37197600
O	0.81635000	-0.02282600	-2.04482700
N	-1.04100000	0.10855700	-0.30440400
C	-1.79155700	-1.03286500	-0.34201300
N	0.74895800	2.05281700	-0.18353800
N	1.00192600	-0.00732000	1.79073200
N	0.48209200	-2.04480900	-0.15592500
C	-3.01686100	1.46884800	-0.30073100
H	-3.51320300	2.43720100	-0.33575700
C	-1.63712600	1.34609100	-0.35537200
C	-0.65421000	2.44561600	-0.64457600
H	-0.60294700	2.57056300	-1.73738300
H	-0.93884700	3.41378600	-0.20528300
C	1.75017300	2.80597300	-1.03192200
H	1.56597200	3.88959800	-0.96802300
H	2.76104100	2.59066300	-0.67258500
H	1.65338400	2.46673300	-2.06848200
C	0.94166700	2.40132600	1.29193100
H	2.02099100	2.51219400	1.45665900
H	0.47760500	3.37742500	1.50559300
C	0.36640100	1.30783900	2.19003300
H	-0.72105600	1.22163900	2.07352300
H	0.57274100	1.53568500	3.24921200
C	2.38130200	-0.08984500	2.40436300
H	2.29867200	-0.07516300	3.50288300
H	2.88348000	-1.01118100	2.09594800
H	2.99569900	0.75515100	2.08103500
C	0.20729700	-1.22624200	2.20880700
H	0.38815800	-1.46510800	3.27022400
H	-0.86097200	-1.00385100	2.09537600
C	0.63549300	-2.39534800	1.32355600
H	0.05339600	-3.30262400	1.55172000
H	1.69293800	-2.63938600	1.48679300
C	1.37448200	-2.93113400	-0.99717800
H	1.31753400	-2.59505500	-2.03775600
H	2.40621700	-2.84172000	-0.64381700
H	1.05410100	-3.98160100	-0.91829800
C	-3.81248700	0.29175600	-0.23616800
C	-3.18459000	-0.98057900	-0.29026000
H	-3.76626600	-1.89968200	-0.32090600
C	-0.96234900	-2.25934100	-0.60665800
H	-1.36943100	-3.17200600	-0.14492800
H	-0.93320900	-2.41489200	-1.69647600
O	-5.15206500	0.50218200	-0.16193700

C	-6.10590900	-0.64189400	-0.14560100
H	-7.08568900	-0.16642500	-0.07363100
H	-6.02663600	-1.21117800	-1.08131300
H	-5.92304800	-1.27441600	0.73345200
N	2.81727600	-0.13942600	-0.48210500
C	3.94441800	-0.21206100	-0.80736300
C	5.32839800	-0.30036600	-1.23651700
H	5.78582400	-1.24636600	-0.90999300
H	5.38644100	-0.25356400	-2.33506000
H	5.92523700	0.52815000	-0.82654300

Hypothetical [(MeO-PyNMe$_3$)Fe^V(O)(MeCN)]$^{3+}$ Cis

Fe	0.83604600	-0.01013500	-0.41302500
O	0.89731900	-0.16700000	-2.03299000
N	-1.04620900	0.11881100	-0.31140900
C	-1.80479200	-1.03559400	-0.35896900
N	0.75271300	2.05820300	-0.18065600
N	1.02436700	-0.04321200	1.75734000
N	0.45610800	-2.05772200	-0.15859500
C	-3.02062700	1.48465500	-0.25196200
H	-3.51968600	2.45347300	-0.25626700
C	-1.64196100	1.36600100	-0.31860500
C	-0.66919300	2.48319600	-0.56280900
H	-0.66304800	2.70855500	-1.64155200
H	-0.93252600	3.41126400	-0.03391700
C	1.73162800	2.81422200	-1.06721500
H	1.56843600	3.89631800	-0.94445400
H	2.75495000	2.57219100	-0.76966000
H	1.57231300	2.53307000	-2.11328600
C	1.03537700	2.37541500	1.29382200
H	2.12471800	2.43501000	1.40542900
H	0.62950100	3.37107300	1.53222900
C	0.44405000	1.29897600	2.19092900
H	-0.64997900	1.25107600	2.11582300
H	0.69474500	1.49376800	3.24608900
C	2.41637300	-0.18022400	2.35116800
H	2.33427900	-0.20148600	3.44864800
H	2.89314200	-1.10317400	2.01183900
H	3.04556200	0.66391600	2.05926000
C	0.19046600	-1.23047400	2.19929600
H	0.37898300	-1.45780200	3.26080200
H	-0.87151900	-0.97439400	2.09844200
C	0.58018400	-2.41672300	1.32730500
H	-0.04528000	-3.29720200	1.54054700
H	1.62201100	-2.71176200	1.50079000
C	1.37587000	-2.94883200	-0.97809700
H	1.31002700	-2.66569700	-2.03406200
H	2.40471900	-2.82972300	-0.62661700
H	1.07338400	-3.99984300	-0.85188200
C	-3.82034800	0.29957100	-0.21881700
C	-3.19256300	-0.98066600	-0.30069500
H	-3.77951600	-1.89639900	-0.35569500
C	-0.97936100	-2.25649900	-0.64772400
H	-1.39400400	-3.17889400	-0.21485300
H	-0.93483300	-2.39166300	-1.74075200
O	-5.14415500	0.51792200	-0.14710500
C	-6.18052800	-0.57280700	-0.13196000

H	-7.11954700	-0.02961900	-0.01459200
H	-6.15293900	-1.10381200	-1.09343500
H	-5.99921500	-1.23996900	0.72097600
N	2.82807800	-0.09166000	-0.46579800
C	3.95780900	-0.15753600	-0.78657100
C	5.34732400	-0.23715400	-1.18395400
H	5.83197400	-1.13081800	-0.75958200
H	5.42789000	-0.29346600	-2.28201900
H	5.90930700	0.64806200	-0.84587300

Hypothetical [(MeO-PyNMe$_3$)Fe^V(O)(MeCN)]$^{3+}$ Trans

Fe	1.17487800	0.06572500	0.08271000
N	-0.77867500	0.10757500	-0.08498700
C	-1.57382700	-0.07351300	1.02732000
O	2.78217900	0.13743900	0.30670000
N	1.05458700	0.22784900	-1.99670500
N	1.27871800	-1.96087400	-0.23047800
N	0.68522300	-0.40987400	2.06347000
C	-2.71475400	0.37301200	-1.48751000
H	-3.18686000	0.56344800	-2.45114800
C	-1.34061100	0.39205900	-1.31540800
C	-0.32073500	0.80206000	-2.34315200
H	-0.22845300	1.89906300	-2.33106500
H	-0.59725200	0.50974600	-3.36728100
C	2.13486500	1.12138900	-2.59066400
H	2.03421400	1.13220500	-3.68700400
H	3.12089000	0.73579500	-2.31450800
H	2.02252000	2.13911900	-2.20669400
C	1.21152300	-1.19280100	-2.56540800
H	2.28215700	-1.35424800	-2.73929300
H	0.71290600	-1.24964200	-3.54485600
C	0.64443900	-2.21383700	-1.59288700
H	-0.44469900	-2.13174100	-1.49008100
H	0.87627600	-3.23871400	-1.92307000
C	2.71364400	-2.48808700	-0.24018500
H	2.68751400	-3.56842600	-0.44479700
H	3.19439100	-2.30853500	0.72458200
H	3.30421200	-1.98474200	-1.01023200
C	0.51495900	-2.61734900	0.91062200
H	0.75637300	-3.69116700	0.94782400
H	-0.56013800	-2.52242800	0.70909900
C	0.92349300	-1.92090000	2.19604100
H	0.36605700	-2.30428000	3.06427100
H	1.99049100	-2.05840900	2.40768000
C	1.54640300	0.32030700	3.08450100
H	1.38547300	1.39832200	2.99406700
H	2.60066200	0.09169500	2.90008200
H	1.26673700	-0.00660000	4.09779800
C	-3.54991300	0.09584600	-0.35715600
C	-2.96098300	-0.10297300	0.92820200
H	-3.57634400	-0.24409500	1.81563900
C	-0.78589700	-0.07095800	2.31197600
H	-1.19680900	-0.75366500	3.07125700
H	-0.82054400	0.94412200	2.73817600
O	-4.86613500	0.07878400	-0.62604700

C	-5.93286800	-0.19149400	0.40010100
H	-6.85393600	-0.19403700	-0.18496200
H	-5.93802400	0.62601700	1.13371300
H	-5.75583800	-1.17038800	0.86450900
N	1.08170000	2.04141500	0.34349200
C	1.22927300	3.19564100	0.51509100
C	1.42483000	4.61529900	0.72300100
H	0.49220900	5.17615000	0.55468500
H	1.76554300	4.81604900	1.75144300
H	2.19117600	5.00591900	0.03404200

Hypothetical [(MeO-PyNMe$_3$)Fe^V(O)]$^{3+}$

Fe	-0.94321300	0.02956000	-0.44622700
O	-1.23368600	0.04313700	-2.00566300
N	0.77190900	-0.11201400	0.12213600
C	1.55341700	1.04873000	0.18824100
N	-1.02007800	-2.02475300	-0.24932000
N	-2.46102500	0.16259600	0.79004300
N	-0.67391300	2.06644300	-0.26862000
C	2.71692700	-1.51994300	0.22418100
H	3.20547000	-2.49279400	0.28457900
C	1.34899400	-1.38877100	0.19178200
C	0.32025400	-2.47315500	0.36406800
H	0.62553400	-3.42641300	-0.08879300
H	0.17170700	-2.65433200	1.44144600
C	-1.21794900	-2.74992800	-1.58084100
H	-1.33126400	-3.82699600	-1.38582800
H	-2.11228500	-2.36902200	-2.08311100
H	-0.34613700	-2.58298400	-2.22258200
C	-2.20041600	-2.31073800	0.69113500
H	-3.08384300	-2.48673700	0.06462100
H	-2.01874400	-3.23850900	1.25521400
C	-2.39103700	-1.12346900	1.62968300
H	-1.55256500	-1.01377100	2.33320000
H	-3.31716400	-1.21865300	2.21911600
C	-3.79152700	0.26113600	0.04267100
H	-4.59928600	0.31555000	0.78836300
H	-3.81379200	1.15717100	-0.58357500
H	-3.94109600	-0.61670100	-0.59187100
C	-2.18944700	1.43500100	1.60847100
H	-3.09284300	1.69050400	2.18545300
H	-1.38748100	1.20273900	2.32475000
C	-1.79981400	2.55812500	0.65225500
H	-1.47630200	3.45535000	1.20215500
H	-2.63631500	2.86203600	0.01111000
C	-0.73110800	2.79759000	-1.61071900
H	0.10730800	2.47794900	-2.23898500
H	-1.67043900	2.56506400	-2.12142600
H	-0.66518600	3.88101200	-1.43022100
C	3.54168400	-0.34066700	0.19601400
C	2.93000600	0.96081200	0.22177100
H	3.53639400	1.86377200	0.28694700
C	0.71496800	2.28827100	0.35625400
H	0.58979300	2.48491200	1.43422000
H	1.17574800	3.18149300	-0.08761400
O	4.84869200	-0.57700900	0.18433700

C	5.92753600	0.48614700	0.15366300
H	6.84820100	-0.09683400	0.09775000
H	5.79396800	1.10642700	-0.74118400
H	5.88094000	1.06143500	1.08733800

References

[1] a) P. Frodevaux, J. M. Harrowfield, A. N. Sobolev, *Inorg. Chem.* **2000**, 39, 4678-4687. b) L. Pellegatti, J. Zhang, B. Drahos, S. Villette, F. Suzenet, G. Guillaumet, S. Petoud, É. Tóth, *Chem. Commun.*, **2008**, 6591-6593.

[2] T. Vermonden, D. Branowska, A. T. M. Marcelisa, E. J. R. Sudhölter, *Tetrahedron*. **2003**, *59*, 5039–5045.

[3] J. Serrano-Plana, A. Aguinaco, R. Belda, E. García-España, M. G. Basallote, A. Company, M. Costas, *Angew. Chem. Int. Ed*. **2016**, *55*, 6310 –6314.

[4] Gary J. Bridger, Sreenivasan Padmanabhan, Renato T. Skerlj, US5698546 A.

[5] Bruker Advanced X-ray Solutions. SMART: Version 5.631, **1997-2002**

[6] Bruker Advanced X-ray Solutions. SAINT +, Version 6.36A, **2001**

[7] a) G. M. Sheldrick, Empirical Absorption Correction Program, Universität Göttingen, **1996**. b) Bruker Advanced X-ray Solutions. SADABS Version 2.10, **2001**.

[8] a) G. M. Sheldrick, Program for Crystal Structure Refinement, Universität Göttingen, **1997**. b) Bruker Advanced X-ray Solutions. SHELXTL Version 6.14, **2000-2003**. SHELXL-2014/7 (Sheldrick, 2014)

[9] Serrano-Plana, J., Oloo, W. N., Acosta-Rueda, L., Meier, K. K., Verdejo, B., García-España, E., E., Basallote, M.G., Münck, E., Que, L., Company, A. and Costas M. *J. Am. Chem. Soc*., **2015**, *137*, 15833–15842.

[10] a) Griffith J. S *Mol Phys.* **1971**, 21, 135–139. b) Taylor CPS. *Biochim Biophys Acta.* **1977**, 491, 137–149. c) Oosterhuis WT, Lang G. *Phys Rev.* **1969**, 178, 439–456.

[11] Oloo, W. N., Meier, K. K., Wang, Y., Shaik, S., Münck, E., & Que, L. *Nat. Commun.*, **2014**, *5*, 3046.

[12] Tiago de Oliveira F, Chanda A, Banerjee D, Shan X, Mondal S, Que L, Bominaar EL, Münck E, Collins TJ. *Science*. **2007**, *315*, 835-8.

[13] Westre, T. E.; Kennepohl, P.; DeWitt, J. G.; Hedman, B.; Hodgson, K. O.; Solomon, E. I. *J. Am. Chem. Soc.* **1997**, *119*, 6297.

[14] George, G. N., EXAFSPAK: A Suite of Computer Programs for Analysis of X-ray Absorption Spectra, **1990**.

[15] Ankudinov, A. L.; Ravel, B.; Rehr J. J.; Conradson, S. D. *Phys. Rev. B* **1998**, *58*, 7565–7576.

[16] Wojdyr, M., *J. Appl. Cryst*., **2010**, *43*, 1126-1128.